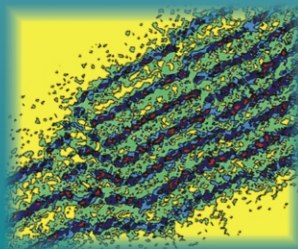
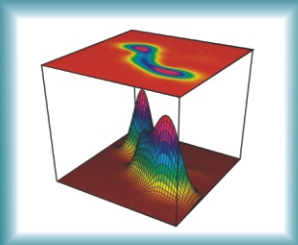
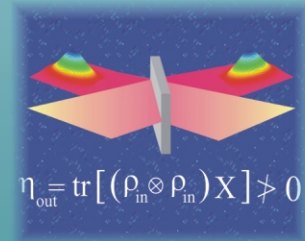
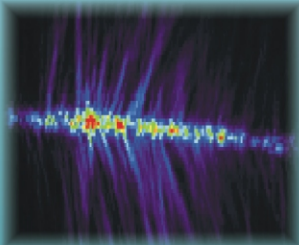
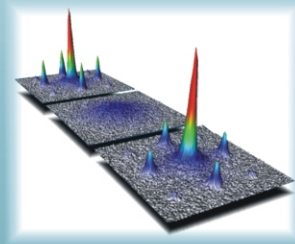
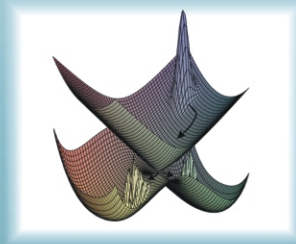


MAX-PLANCK-INSTITUT FÜR QUANTENOPTIK

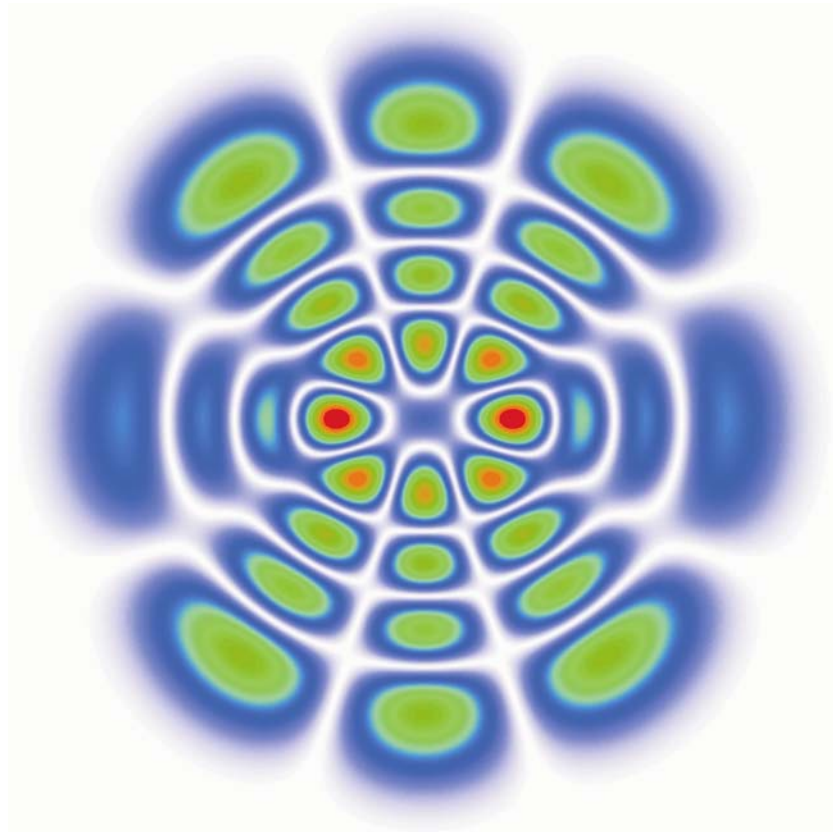


PROGRESS REPORT
2001/2002

Hans-Kopfermann-Str.1, D-85748 GARCHING

1.4 QUANTUM DYNAMICS DIVISION

G. Rempe



SCIENTIFIC STAFF:

S. Dürr (since November 2001), A. Kuhn, S. Rangwala (since September 2001), P.W.H. Pinkse

PH.D. CANDIDATES:

T. Fischer, M. Hennrich, M. Hijlkema, T. Junglen, T. Legero, A. Marte, P. Maunz, S. Nußmann, T. Puppe, T. Rieger, J. Schuster*, T. Wilk
(* received Ph.D. during report period)

DIPLOMA CANDIDATES:

S. Amtage*, S. Ernst, P. Krok, S. Kudera*, T. Rieger*, F. Rohde, B. Sang*, I. Schuster, T. Volz, B. Weber, S. Wöbner*
(* received Diploma during report period)

SCIENTIFIC GUESTS:

H.C.W. Beijerinck, P. Horak, H. Ritsch, B.W. Shore, B.J. Verhaar

1.4.1 SUMMARY OF SCIENTIFIC ACTIVITIES

Three years after moving to the Max-Planck Institute, all experiments in the Quantum Dynamics division are operational. Our research now focuses on

- Bose-Einstein condensation,
- Cavity Quantum Electrodynamics,
- Quantum Information, and
- Slow Molecules.

The following pages briefly summarize the main results achieved during the last 2 years. A selection of reprints is presented at the end.

1.4.1.1 BOSE-EINSTEIN CONDENSATION

The realization of Bose-Einstein condensation in dilute gases in 1995 [1] was a milestone in the rapidly developing field of cooling and trapping of atoms. One important aspect of Bose-Einstein condensation in atomic gases is the role of interactions among the atoms. Under typical experimental conditions, this interaction is weak and, hence, can be treated in terms of a mean-field approach. For high density, however, this approximation breaks down. In this collisional (hydrodynamic) regime, a rich variety of interesting effects beyond the mean-field approximation emerges. This collisional regime can be approached in two different ways. One is to increase the density. However, our experiment revealed density-limiting avalanche losses, as discussed below [2]. Besides increasing the density, another possible approach is to increase the interaction among the atoms by means of a Feshbach resonance [3]. A large number of Feshbach resonances in rubidium 87 have very recently been observed in our experiment and are still under investigation.

AVALANCHES IN A BOSE-EINSTEIN CONDENSATE

Last year we focused our activities on the study of surprisingly fast losses observed in a rubidium 87 condensate with a high density. Losses due to inelastic collisions are unavoidable in dilute-gas BEC experiments since the thermodynamic ground state of the system at low temperatures is usually a solid. As a first step towards a solid, molecules are formed in inelastic collisions. These molecules are typically in a highly excited vibrational state, and the binding energy is released as kinetic energy of the involved particles. At low density, these particles have a sufficiently large energy to leave the trap. Such a particle loss is observed in any BEC experiment. At high density, however, the particles

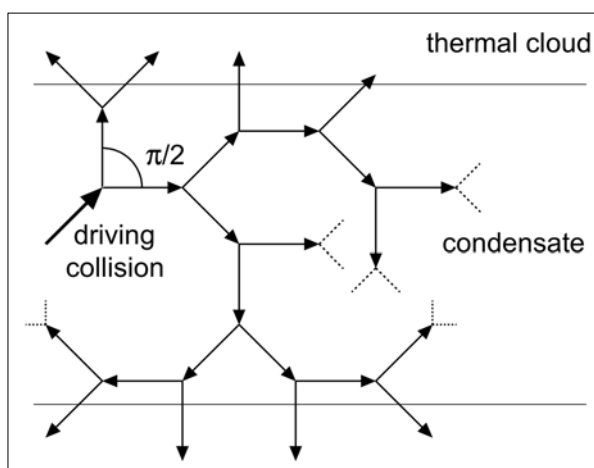


Fig. 1: Sketch of a collisional avalanche in a Bose-Einstein condensate. If the mean free path for inelastic decay products is small compared to the size of the condensate, further collisions lead to a significantly enhanced loss rate.

resulting from the recombination process can undergo secondary collisions with other atoms. The reason for this is the large collisional cross section at the low velocities involved. Before leaving the condensate, the moving particles can therefore transfer energy to condensate atoms. This, in turn, leads to additional atom loss. For very high density, even atoms involved in secondary collisions will undergo further collisions before leaving the trap. In this regime, a single inelastic collision can trigger a collisional avalanche leading to dramatically enhanced loss (Fig. 1).

For example, in our experiment this results in an 8-fold increase of the initial loss rate. We developed a model accounting for avalanche losses, which is in good agreement with the observed decay of the condensate. This analysis reveals that the so-called collisional opacity of an ultra-cold and dense gas exhibits a critical value. When the critical opacity is exceeded, losses induced by inelastic collisions are substantially enhanced.

1.4.1.2 CAVITY QUANTUM ELECTRODYNAMICS

In 2000 we achieved trapping of a single cold atom in a high-finesse cavity containing about one photon on average [4]. We have continued to study this textbook example of matter-light interaction. For example, to track the motion of the atom, we proposed a novel detection technique, "the atomic kaleidoscope" [5]. This activity was done in cooperation with Peter Horak and Helmut Ritsch from the University of Innsbruck, Austria. Simultaneously, the description of the motion

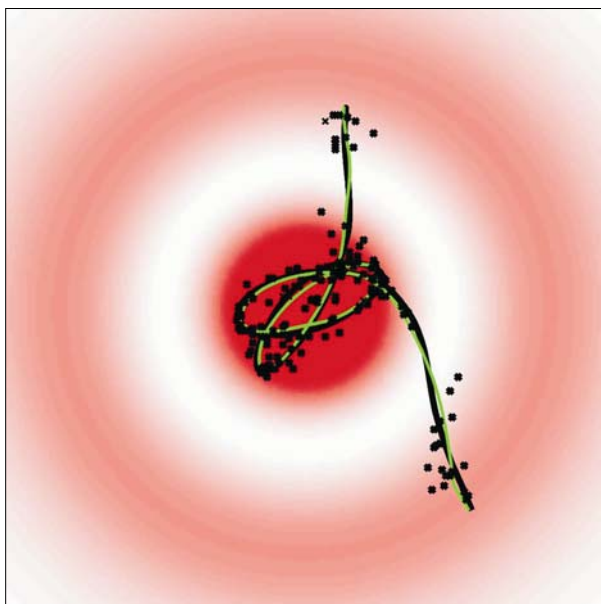


Fig. 2: Reconstruction of a simulated trajectory. Photon clicks in 16 segments of a detector were determined during a computer-simulated atomic trajectory (black curve). The detector clicks were used to estimate the atomic position (crosses). The green curve was obtained by a spline interpolation of the crosses. The picture measures $(90 \mu\text{m})^2$, the empty-cavity mode is indicated in red.

of a single atom in a single-mode cavity was generalized to describe the motion of many atoms in many modes [6]. Besides these theoretical activities, we have successfully extended the storage time of the atom in the cavity by employing feedback techniques [7].

THE ATOMIC KALEIDOSCOPE

The phase shift and loss induced by a single atom can significantly influence the light intensity inside a high-finesse cavity. These effects depend on the electric field strength at the position of the atom and, hence, on the spatial dependence of the cavity mode function. The transmission of the cavity can therefore be used to deduce information on the position of the atom. In the case of an axial symmetric fundamental Gaussian beam, only the radial distance to the cavity axis can be measured. Nevertheless, if angular momentum is conserved, it is possible to reconstruct the trajectory of the atom by modelling the potential for the atom [8]. A reconstruction that does not rely on modelling is possible if frequency-degenerate higher-order transverse modes are used. It exploits the fact that an atom redistributes photons between near-degenerated modes,

and changes their relative phases such that the transmitted spatial intensity pattern will show a local maximum or minimum near the transversal position of the atom. By analogy with the beautiful symmetric patterns of a toy kaleidoscope, we call this method the atomic kaleidoscope. We have demonstrated the potential of the method by reconstruction of a computer-generated trajectory of an atom in a cavity sustaining a set of Laguerre-Gaussian modes [5]. Calculating the cavity field patterns, and hence, estimating the position of the atom given some output pattern is simplified by the introduction of the “effective mode” [9]. From the estimated positions of the atom, a trajectory could be reconstructed without relying on knowledge about the forces acting on the atom (Fig. 2).

FEEDBACK ON THE MOTION OF A SINGLE ATOM

The principle of feedback is a common and very general technique to stabilize a system against perturbations. Feedback can also provide a way to control the motion of a single neutral atom. It requires a position measurement with high spatial and temporal resolution and a large feedback bandwidth. All these requirements can be fulfilled using a high-finesse cavity.

In detail, the presence and the motion of the atom is monitored by observing the cavity transmittance. First, the light intensity is suddenly switched to a higher value when an atom is detected in the cavity. In this way, the atom can be trapped in a potential well that is deeper than the one it fell into [4]. Second, continuous feedback is applied while the stored atom moves inside the cavity (Fig. 3). Different feedback strategies

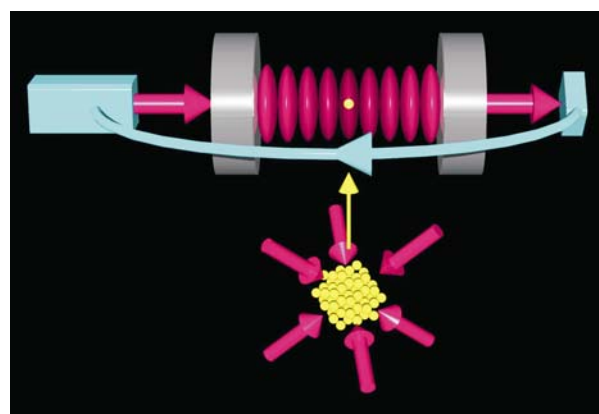


Fig. 3: A continuous feedback loop uses the information in the light transmitted by the cavity to influence the motion of the atom by altering the power of the injected laser light. In this way, the time an atom can be kept in the cavity can be prolonged.

are employed, depending on a position or velocity measurement. While moving in the cavity light field, the atom experiences random momentum kicks from spontaneous emission events. Eventually, this leads to the escape of the atom. By decreasing the light intensity when the atom resides near the trap center, heating of the atom is suppressed. Despite severe limitations from detection noise, the random character of the atomic motion and the shallow optical potential, the feedback considerably extends the time the atom spends in the cavity [7].

1.4.1.3 QUANTUM INFORMATION

Our projects in quantum information processing are aiming at the realization of basic building blocks for future quantum computers and quantum networks using ultra-cold trapped neutral atoms. Most of these activities rely on strongly coupled atom-cavity systems and employ a controlled energy exchange between the atom and the quantized light field of a cavity. This is done in form of an adiabatic passage [10] driving a Raman transition in a three-level atom. The two lower lying atomic levels are non-decaying ground states of the atom. One of them is coupled to the third, electronically excited atomic level by a laser pulse, while the cavity couples the excited level to the other atomic ground state. The Raman transition from one ground state to the other goes hand-in-hand with a change of the photon number in the cavity. This process is unitary and therefore reversible, so that it should allow one to map the state of an atom to a photon and vice versa, which is the starting point for distributed quantum networking [11]. Moreover, the system can operate as a deterministic source of indistinguishable single photons, which are an essential prerequisite for all-optical quantum information processing [12].

VACUUM-STIMULATED RAMAN SCATTERING

Three years ago, we have proposed to drive a Raman transition in a single atom coupled to a cavity to produce single photons [13]. Along this line, we have demonstrated that this process is physically feasible [14]: Single Rubidium

atoms released from a magneto-optical trap pass through an empty high-finesse cavity, resonant with one branch of the Raman transition of the atom. A laser beam that excites the other branch of the Raman transition crosses the cavity slightly downstream with respect to the atomic motion. This assures that every single falling atom experiences a so-called counter-intuitive interaction sequence, where it first sees the cavity and then the laser beam. As a result, the quantum state of the atom-cavity system adiabatically follows an evolution that, in the end, leads to the emission of a photon from the cavity for every atom falling through [15]. Although this process is not controlled and only maps the random atom statistics to the photons, it allows a spectroscopic investigation of the underlying Raman process.

As expected, we found that photons are emitted only if the Raman-resonance condition is fulfilled, i.e. with cavity and laser beam detuned by the same amount from the respective atomic transition. Moreover, the observed spectral lines are of subnatural width, which underpins the Raman nature of the photon generation process, and excludes effects such as enhanced spontaneous emission, where an atom would be first electronically excited, and then would emit into the cavity with an enhanced probability. In such a case, much broader lines would be found on the atomic resonance.

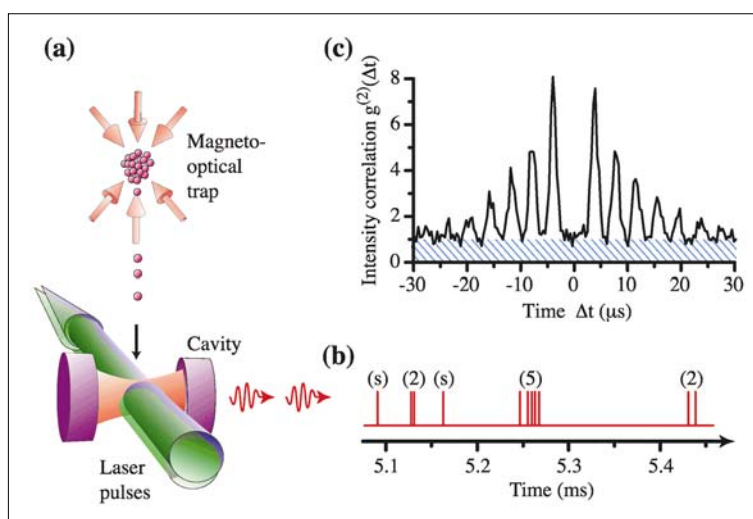


Fig. 4: Experimental setup of the single-photon source. (a) Atoms collected and released from a magneto-optical trap fall through a high-finesse optical cavity, where they are exposed to a sequence of laser pulses that trigger single-photon emissions. The photon emissions (b) are recorded as a function of time. Solitary photons (s), pairs (2) and bursts of five (5) are observed. The intensity-correlation of the photons (c) shows that the pulses trigger photon emissions, and that photons are emitted one-by-one.

We have also investigated the photon emission probability as a function of the laser beam displacement from the cavity axis. As a clear signature of adiabatic following, the peak of the emission probability is found in case of a counter-intuitive interaction sequence. The number of observed emissions drops significantly if the atoms are first excited by the laser and stimulated by the cavity at a later moment.

SINGLE PHOTONS ON DEMAND

Recently, we extended our scheme to produce sequences of single photons on demand. We therefore realized a pulsed excitation scheme where an atom is exposed to an alternating sequence of pump laser pulses, triggering single-photon emissions, and recycling laser pulses, resonant with the cavity-branch of the Raman transition. By means of optical pumping, these recycling pulses re-establish the initial atomic state, so that successive photon emissions are possible. Indeed, sequences of up to seven single photons on demand are observed while a single atom interacts with the cavity [16]. The duration of these sequences is only limited by the finite atom-cavity interaction time.

QUANTUM GATES AND NETWORKS

Quantum networking in a distributed network of coupled atom-cavity systems [11] requires single atoms permanently interacting with a single mode of the surrounding cavity, so that the quantum state of an atom can be mapped onto the state of a photon and then to another atom in a controlled way. Moreover, the photons which are emitted from such a permanently coupled atom-cavity system are expected to be indistinguishable, so that they can also be used for all-optical quantum information processing with linear components [12].

With these promising perspectives in view, we started to implement an improved version of the above experiment. The new setup will allow triggering many successive single-photon emissions in a controlled way, while a single atom is held at rest in the cavity. Therefore, a magneto-optical surface trap has been realized, which is used to fill a red-detuned dipole trap with a small number of Rubidium atoms. This latter trap will allow guiding and holding an atom between the cavity mirrors.

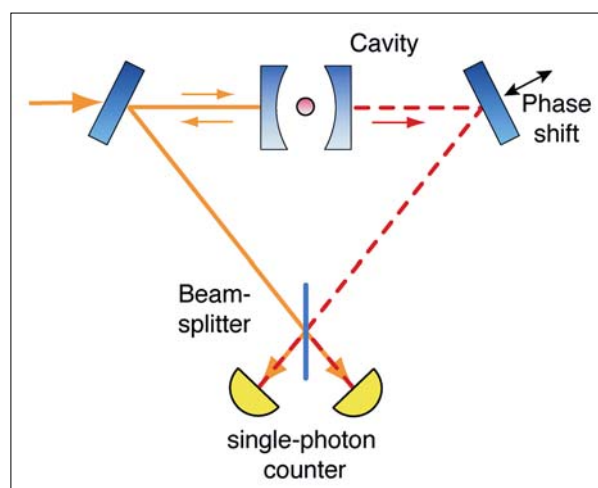


Fig. 5: Mach-Zehnder Interferometer using an optical high-finesse cavity in place of a first beam splitter. The phase difference between the two paths is expected to be so sensitive to the presence of a single atom in the cavity, that correlations between the observed fringes and the atomic state will reveal atom-photon entanglement.

ENTANGLEMENT IN CAVITIES

Quantum gate operations in optical cavities are based on the entanglement of single atoms, carrying qubits, and the photon-number state of the cavity. To investigate the entanglement of a single atom with the light field in a future experiment, we have installed a Mach-Zehnder interferometer that makes use of a cavity in place of its first beam splitter. This cavity should be able to entangle all photons impinging on one of its mirrors with a single atom located in the cavity. So far, the interferometer has been characterized without atoms: We observe that the relative phase between the two interferometer paths changes when the detuning of the light changes from red to blue with respect to the cavity resonance, and we obtain a fringe visibility of about 80% at both output ports of the interferometer. An atom in the cavity can lead to comparable detunings, so that the phase difference observed with the interferometer is expected to correlate with the atomic state (Fig. 5).

1.4.1.4 SLOW MOLECULES

Recent advances in physics with dilute, cold atoms has generated great interest in the cooling and trapping of molecules [17]. As compared to atoms, molecules have a complex internal structure, giving rise to rotational

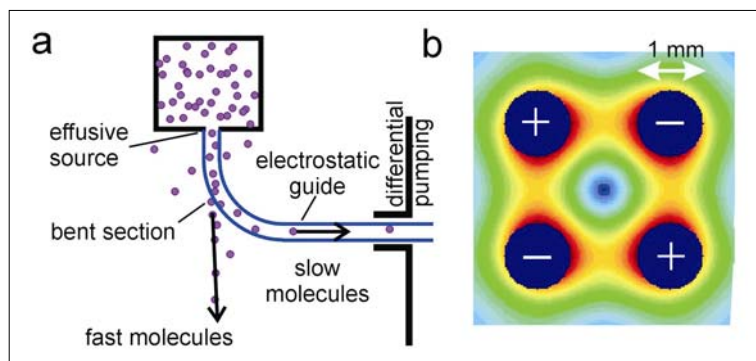


Fig. 6: Setup of the cold-molecules source. a) Thermal, polar, molecules are injected in the quadrupole guide. Whereas the fast molecules escape, the slow low-field seeking molecules are guided around the bend, through the differential pumping section into a detector. b) Cross section of the quadrupole guide. The colours indicate the electric field strength, red is high, blue is low.

and vibrational motion about their centre of mass and can in addition exhibit a permanent dipole moment. Trapping cold molecules will potentially lead to new physics due to the internal molecular dynamics and the long range and anisotropy of the dipole-dipole interactions. The objective of the cold molecule project is to explore this new field and to develop paths for achieving cold molecular samples. Since molecules cannot be laser cooled for want of closed optical transitions, the creation of a population of cold molecules requires new techniques (Fig. 6).

Our source relies on the fact that enough slow molecules are present in any thermally distributed gas, even at room temperature. They only need to be filtered out. We exploit the Stark interaction of polar molecules with an inhomogeneous, electrostatic field to select slow molecules from a room-temperature effusive source. In contrast to other techniques for the production of cold molecules, our method produces a continuous flux of slow molecules, which is conveniently delivered into an ultra-high vacuum. Its main advantage, however, is its simplicity and versatility.

The project started with an empty lab in spring of 2001. At the moment of writing, a first version of the source has successfully been set up that produces a beam of slow formaldehyde (H_2CO) molecules.

REFERENCES

- [1] M. Anderson et al., *Science* **269**, 198 (1995); K. Davis et al., *Phys. Rev. Lett.* **75**, 3969 (1995); C. Bradley et al., *Phys. Rev. Lett.* **75**, 1687 (1995).
- [2] J. Schuster et al., *Phys. Rev. Lett.* **87**, 170404 (2001).
- [3] S. Inouye et al., *Nature* **392**, 151 (1998); P. Courteille et al., *Phys. Rev. Lett.* **81**, 69 (1998); J. Roberts et al., *Phys. Rev. Lett.* **81**, 5109 (1998); V. Vuletic et al., *Phys. Rev. Lett.* **82**, 1406 (1999); T. Loftus et al., *Phys. Rev. Lett.* **88**, 173201 (2002); L. Khaykovich et al., *Science* **296**, 1290 (2002).
- [4] P.W.H. Pinkse et al., *Nature* **404**, 365 (2000).
- [5] P. Horak et al., *Phys. Rev. Lett.* **88**, 043601 (2002).
- [6] T. Fischer et al., *Phys. Rev. Lett.* **88**, 163002 (2002).
- [7] T. Fischer et al., *New Journal of Physics* **3**, 11.1 (2001).
- [8] C.J. Hood et al., *Science* **287**, 1447 (2000).
- [9] P. Maunz et al., submitted
- [10] N.V. Vitanov et al., *Adv. At. Mol. Opt. Phys.* **46**, 55-190 (2001).
- [11] J.I. Cirac et al., *Phys. Rev. Lett.* **78**, 3221-3224 (1997).
- [12] E. Knill et al., *Nature* **409**, 46-52 (2001).
- [13] A. Kuhn et al., *Appl. Phys. B* **69**, 373-377 (1999).
- [14] M. Hennrich et al., *Phys. Rev. Lett.* **85**, 4872-4875 (2000).
- [15] A. Kuhn et al., *Varenna Lecture Notes*, (in print).
- [16] A. Kuhn et al., *Phys. Rev. Lett.* **89**, 067901 (2002).
- [17] J.D. Weinstein et al., *Nature* **395**, 148-150 (1998); H.L. Bethlem et al., *Nature* **406**, 491-494 (2000).

1.4.2 SURVEY OF THE RESEARCH ACTIVITIES

PROJECT	OBJECTIVE	STAFF
Bose-Einstein Condensation		
Collisional avalanches	Investigation of fast losses from a dense Bose-Einstein condensate due to collisional avalanches	S. Amtage, A. Marte, B. Sang, J. Schuster, S. Wöbner
Feshbach resonances	Control of atomic collision properties	S. Dürr, S. Ernst, A. Marte, J. Schuster, T. Volz
Cavity Quantum Electrodynamics		
Feedback control	Controlling the motion of a single atom in a high finesse cavity by means of feedback	T. Fischer, P. Maunz, P.W.H. Pinkse T. Puppe, I. Schuster
Optical kaleidoscope	Development of a new observation technique for single atoms with high spatial resolution employing higher-order modes of a high-finesse cavity	T. Fischer, P. Maunz, P.W.H. Pinkse T. Puppe,
Quantum Information		
Vacuum-stimulated Raman scattering	Stimulated Raman adiabatic passage with the vacuum field of a cavity acting in place of a stimulating laser	M. Hennrich, A. Kuhn, T. Legero
Single photons on demand	Controlled emission of indistinguishable single-photon pulses from a single atom strongly coupled to a high-finesse optical cavity	M. Hennrich, P. Krok, A. Kuhn, T. Legero, T. Wilk
Quantum gates and networks	All-optical quantum gates acting on indistinguishable single photons travelling from node to node in a distributed quantum network of atom-cavity systems	M. Hijlkema, A. Kuhn, S. Nußmann, F. Rohde, B. Weber
Entanglement in cavities	Entanglement of a single atom with the photon number state in an optical cavity	S. Kudera, A. Kuhn, T. Legero
Slow Molecules		
Stark guide	Creation of a high-flux beam of slow molecules exploiting the Stark effect in polar molecules	T. Junglen, P.W.H. Pinkse, S. Rangwala, T. Rieger

1.4.3 SELECTED REPRINTS

S. Dürr and G. Rempe:

Can wave-particle duality be based on the uncertainty relation?

American Journal of Physics **68**, 1021-1024 (2000)

M. Hennrich, T. Legero, A. Kuhn, and G. Rempe:

Vacuum-Stimulated Raman Scattering Based on Adiabatic Passage in a High-Finesse Optical Cavity.

Phys. Rev. Lett. **85**, 4872-4875 (2000)

J. Schuster, A. Marte, S. Amthar, B. Sang, and G. Rempe:

Avalanches in a Bose-Einstein Condensate.

Phys. Rev. Lett. **87**, 170404 (2001)

P. Horak, H. Ritsch, T. Fischer, P. Maunz, T. Puppe, P.W. H. Pinkse, and G. Rempe:

Optical Kaleidoscope Using a Single Atom.

Phys. Rev. Lett. **88**, 043601 (2002)

T. Fischer, P. Maunz, P.W.H. Pinkse, T. Puppe, and G. Rempe:

Feedback on the Motion of a Single Atom in an Optical Cavity.

Phys. Rev. Lett. **88**, 163002 (2002)

A. Kuhn, M. Hennrich, and G. Rempe:

Deterministic Single-Photon Source for Distributed Quantum Networking.

Phys. Rev. Lett. **89**, 067901 (2002)

Can wave–particle duality be based on the uncertainty relation?

Stephan Dürr and Gerhard Rempe^{a)}

Max-Planck-Institut für Quantenoptik, Hans-Kopfermann-Strasse 1, 85748 Garching, Germany

(Received 28 July 1999; accepted 27 January 2000)

Wave and particle properties of a quantum object cannot be observed simultaneously. In particular, the fringe visibility in an interferometer is limited by the amount of which-way information which can be obtained. This limit is set by the recently discovered duality relation. So far, all derivations of the duality relation are independent of Heisenberg's uncertainty relation. Here we demonstrate that it is alternatively possible to derive the duality relation in the form of an uncertainty relation for some suitably chosen observables. © 2000 American Association of Physics Teachers.

I. INTRODUCTION

Wave–particle duality refers to the fact that a quantum object can exhibit either wave or particle properties, depending on the experimental situation. In a double-slit experiment, for example, the object must pass through both slits simultaneously in order to create an interference pattern. This testifies to the object's wave nature. On the other hand, performing a which-way experiment reveals which of the slits each object passes through, manifesting its particle nature. However, performing a which-way experiment unavoidably destroys the interference pattern.

This was illustrated in various gedanken experiments, such as Einstein's recoiling slit¹ or Feynman's light microscope.² In order to explain the loss of interference in which-way experiments, one usually invokes Heisenberg's position–momentum uncertainty relation. This has been analyzed in great detail by, e.g., Wiseman *et al.*³ However, Scully, Englert, and Walther⁴ pointed out that such an explanation need not always be possible, but that the entanglement between the which-way marker and the interfering quantum object can always explain the loss of interference. Several experiments support this point of view.^{5–11}

This entanglement need not always be perfect. In general, a measurement performed on the which-way marker yields only incomplete which-way knowledge. In order to quantify how much which-way information is available from such a measurement, one typically uses the “distinguishability,” D . With incomplete which-way information stored, one obtains interference fringes with a reduced visibility, V , which is limited by the so-called duality relation

$$D^2 + V^2 \leq 1. \quad (1)$$

This fundamental limit was recently discovered by Jaeger, Shimony, and Vaidman,¹² and independently by Englert.¹³ It can be regarded as a quantitative statement about wave–particle duality. In the special case, where full which-way information is stored, $D=1$, it implies that the interference fringes are lost completely, $V=0$. The first experimental tests of the duality relation have been performed recently.^{14,15}

Incomplete which-way information can alternatively be obtained without a which-way marker by setting up the interferometer such that the particle fluxes along the two ways differ. In this case, the which-way knowledge is expressed in the form of the so-called “predictability,” P , which is limited by^{12,13,16–20}

$$P^2 + V^2 \leq 1. \quad (2)$$

This result was confirmed experimentally in Refs. 21 and 22.

None of the derivations of Eqs. (1) and (2) cited above involves any form of the uncertainty relation. It therefore seems that “the duality relation is logically independent of the uncertainty relation.”¹³ In this article, we will show, however, that for arbitrary which-way schemes, Eqs. (1) and (2) can always be derived in the form of a Heisenberg–Robertson uncertainty relation for some suitably chosen observables (which will turn out to be different from position and momentum).

II. PREDICTABILITY

In this section, we consider a two-beam interferometer without a which-way marker, as shown in Fig. 1. Let $|+\rangle$ and $|-\rangle$ denote the state vectors corresponding to the two ways along which the object can pass through the interferometer. After passing the first beam splitter, the density matrix in a representation with respect to the basis $\{|+\rangle, |-\rangle\}$ reads

$$\rho = \begin{pmatrix} w_+ & \rho_{\pm} \\ \rho_{\pm}^* & w_- \end{pmatrix}. \quad (3)$$

The probabilities w_+ and w_- that the object moves along one way or the other, respectively, fulfill $\text{Tr}\{\rho\} = w_+ + w_- = 1$. The magnitude of the difference between these probabilities is the predictability

$$P = |w_+ - w_-|, \quad (4)$$

which is obviously determined by the reflectivity of the first beam splitter. P quantifies how much which-way knowledge we have. For $P=0$, corresponding to a 50:50 beam splitter, we have no which-way knowledge, whereas for $P=1$, we know precisely which way the object takes.

Without loss of generality, we assume that the second beam splitter is a 50:50 beam splitter. Taking into account the phase shift φ between the two interferometer arms, the upper output beam corresponds to the state vector $|u_{\varphi}\rangle = (|+\rangle + e^{i\varphi}|-\rangle)/\sqrt{2}$. The intensity in this beam is

$$I_u(\varphi) \propto \langle u_{\varphi} | \rho | u_{\varphi} \rangle = \frac{1}{2}(1 + 2|\rho_{\pm}| \cos(\varphi + \varphi_0)) \quad (5)$$

with $\rho_{\pm} = |\rho_{\pm}| e^{i\varphi_0}$. The visibility of this interference pattern is

$$V = \frac{I_{\max} - I_{\min}}{I_{\max} + I_{\min}} = 2|\rho_{\pm}|, \quad (6)$$

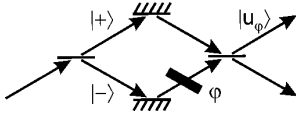


Fig. 1. Scheme of a typical two-beam interferometer. The incoming beam (left) is split into two beams, denoted $|+\rangle$ and $|-\rangle$. After reflection from mirrors, the phase of one of the beams is shifted by φ . Next, the two beams are recombined on a second beam splitter. Due to interference, the intensities of the two outgoing beams vary as a function of the phase shift φ .

where I_{\max} and I_{\min} denote the maximum and minimum intensities. The relation, Eq. (2), limiting visibility and predictability can easily be derived from $\text{Tr}\{\rho^2\} = w_+^2 + w_-^2 + 2|\rho_{\pm}|^2 = \{1 + P^2 + V^2\}/2 \leq 1$.

We will now show that this inequality can alternatively be obtained in the form of a Heisenberg–Robertson uncertainty relation^{23,24}

$$\Delta A \Delta B \geq \frac{1}{2} |\langle [A, B] \rangle|, \quad (7)$$

which applies to each pair of Hermitian operators A and B , with the expectation values and standard deviations of operators defined as $\langle A \rangle = \text{Tr}\{\rho A\}$ and $\Delta A = \sqrt{\langle A^2 \rangle - \langle A \rangle^2}$, respectively.

In order to find suitable operators A and B , we investigate the Pauli spin-matrices

$$\sigma_x = \begin{pmatrix} 0 & 1 \\ 1 & 0 \end{pmatrix}, \quad \sigma_y = \begin{pmatrix} 0 & -i \\ i & 0 \end{pmatrix}, \quad \sigma_z = \begin{pmatrix} 1 & 0 \\ 0 & -1 \end{pmatrix}. \quad (8)$$

Their expectation values are $\langle \sigma_x \rangle = 2 \text{Re}\{\rho_{\pm}\}$, $\langle \sigma_y \rangle = -2 \text{Im}\{\rho_{\pm}\}$, and $\langle \sigma_z \rangle = w_+ - w_-$. Obviously, $\langle \sigma_z \rangle$ reflects our which-way knowledge, whereas $\langle \sigma_x \rangle$ and $\langle \sigma_y \rangle$ are related to the interference pattern via

$$I_u(\varphi) \propto \frac{1}{2} (1 + \cos \varphi \langle \sigma_x \rangle + \sin \varphi \langle \sigma_y \rangle). \quad (9)$$

Without loss of generality, we choose the relative phase between states $|+\rangle$ and $|-\rangle$ such that ρ_{\pm} is real, i.e., $\varphi_0 = 0$. Thus we obtain

$$|\langle \sigma_x \rangle| = V, \quad \langle \sigma_y \rangle = 0, \quad |\langle \sigma_z \rangle| = P. \quad (10)$$

With this choice of the phases, $\langle \sigma_x \rangle$ and $\langle \sigma_z \rangle$ represent the wave character and particle character of the ensemble, respectively. The standard deviations of these observables,

$$\Delta \sigma_x = \sqrt{1 - V^2}, \quad \Delta \sigma_y = 1, \quad \Delta \sigma_z = \sqrt{1 - P^2}, \quad (11)$$

are easily obtained, because $\sigma_x^2 = \sigma_y^2 = \sigma_z^2 = \mathbf{1}$. Using the commutator $[\sigma_j, \sigma_k] = 2i \sum_l \epsilon_{jkl} \sigma_l$, we can now evaluate the uncertainty relation, Eq. (7), for all possible pairs of the above standard deviations, yielding

$$\sqrt{1 - V^2} = \Delta \sigma_x \Delta \sigma_y \geq |\langle \sigma_z \rangle| = P, \quad (12)$$

$$\sqrt{1 - P^2} = \Delta \sigma_y \Delta \sigma_z \geq |\langle \sigma_x \rangle| = V, \quad (13)$$

$$\Delta \sigma_z \Delta \sigma_x \geq |\langle \sigma_y \rangle| = 0. \quad (14)$$

Equation (14) yields a trivial result, because standard deviations are non-negative by definition. However, Eqs. (12) and (13) are equivalent to the desired relation, Eq. (2). Hence, for the case without a which-way marker, Eq. (2) can be derived in the form of an uncertainty relation for the components of an abstract pseudospin.

III. DUALITY RELATION

Let us now add a second quantum system (called which-way marker) to the interferometer. When an object is passing through the interferometer, a suitable interaction shall change the quantum state of the which-way marker depending on the way the object took. This creates an entanglement between the which-way marker and the way of the object. A later measurement on the which-way marker can then reveal which way the object took. In other words, which-way information is now stored in the which-way marker. For simplicity, we assume that the which-way marker does not suffer from decoherence²⁵ (at least as long as we do not couple the marker to a macroscopic “needle”).

Let ρ_{tot} denote the density matrix of the total system (object plus which-way marker) after the interaction (but before the phase shifter and the second beam splitter). Again, we denote the pseudospin corresponding to the ways by σ_x , σ_y , and σ_z . And again, we choose the relative phase between states $|+\rangle$ and $|-\rangle$ such that $\langle + | \text{Tr}_M \{ \rho_{\text{tot}} \} | - \rangle$ is real, where Tr_M denotes the trace over the which-way marker. Thus we reproduce the above results, in particular,

$$|\langle \sigma_x \rangle| = V, \quad \Delta \sigma_x = \sqrt{1 - V^2}. \quad (15)$$

In order to read out the which-way information, we measure an observable W of the which-way marker with eigenvalues $\{w_1, w_2, \dots\}$ and an orthonormal basis of eigenstates $\{|w_1\rangle, |w_2\rangle, \dots\}$. Let $p(\pm, w_i)$ denote the joint probability that w_i is found and that the object moves along way $|\pm\rangle$. If w_i is found, the best guess one can make about the way is to opt for way $|+\rangle$ if $p(+, w_i) \geq p(-, w_i)$, and for way $|-\rangle$ otherwise. This yields the “likelihood for guessing the way right,”¹³

$$L_W = \sum_i \max\{p(+, w_i), p(-, w_i)\}. \quad (16)$$

Since L_W can vary between 1/2 and 1, it is natural to scale this quantity by defining the “which-way knowledge”²⁶

$$K_W = 2L_W - 1 = \sum_i |p(+, w_i) - p(-, w_i)| \quad (17)$$

so that $0 \leq K_W \leq 1$. Obviously, K_W depends on the choice of the measured observable W . In order to quantify how much which-way information is actually stored, the arbitrariness of the read-out process can be eliminated by defining the “distinguishability”^{12,13,26}

$$D = \max_w \{K_W\}, \quad (18)$$

which is the maximum value of K_W that is obtained for the best choice of W . The distinguishability is limited by the duality relation, Eq. (1), which has been derived in Refs. 12 and 13 without using the uncertainty relation.

We will now show that the duality relation—just as Eq. (2)—can alternatively be derived in the form of a Heisenberg–Robertson uncertainty relation for some suitably chosen observables. For that purpose, let

$$\epsilon_i = \begin{cases} +1 & \text{if } p(+, w_i) \geq p(-, w_i) \\ -1 & \text{otherwise} \end{cases} \quad (19)$$

denote which way to bet on if the eigenstate $|w_i\rangle$ is found. Using $p(+, w_i) = \langle w_i + | \rho_{\text{tot}} | w_i + \rangle$, we thus find

$$K_W = \sum_i \epsilon_i (\langle w_i + | \rho_{\text{tot}} | w_i + \rangle - \langle w_i - | \rho_{\text{tot}} | w_i - \rangle) \quad (20)$$

$$= \sum_i \epsilon_i \text{Tr} \{ \rho_{\text{tot}} (| w_i \rangle \langle w_i | \otimes \sigma_z) \}, \quad (21)$$

where we used $\sigma_z = | + \rangle \langle + | - | - \rangle \langle - |$ and where Tr denotes the trace over the total system. Let us define the observable

$$W_\epsilon = \sum_i \epsilon_i | w_i \rangle \langle w_i |. \quad (22)$$

In passing, we note that $W_\epsilon^2 = \mathbf{1}$ and $[\sigma_x, W_\epsilon] = [\sigma_y, W_\epsilon] = [\sigma_z, W_\epsilon] = 0$. Inserting W_ϵ into Eq. (21), we obtain

$$K_W = \langle \sigma_z W_\epsilon \rangle. \quad (23)$$

Note that we are considering a joint observable of the total system (object plus which-way marker) here, which is clearly necessary to explore the correlations between the which-way marker and the way taken by the object.

Let us now choose an observable W_{max} , such that K_W is maximized. For simplicity, we will denote the corresponding observable defined by Eq. (22) by W_0 (instead of $W_{\text{max}, \epsilon}$). Hence, we obtain

$$D = \langle \sigma_z W_0 \rangle. \quad (24)$$

It is easy to see that $\sigma_z W_0$ is Hermitian and that $(\sigma_z W_0)^2 = \mathbf{1}$, so that its standard deviation is

$$\Delta(\sigma_z W_0) = \sqrt{1 - D^2}. \quad (25)$$

Additionally, let us consider the observable $\sigma_y W_0$ which also fulfills $(\sigma_y W_0)^2 = \mathbf{1}$. As it is also Hermitian, its expectation value is real, so that

$$\Delta(\sigma_y W_0) = \sqrt{1 - \langle \sigma_y W_0 \rangle^2} \leq 1. \quad (26)$$

Using the commutator $[(\sigma_y W_0), (\sigma_z W_0)] = 2i\sigma_x$, we can now write down the corresponding uncertainty relation. In combination with Eqs. (15), (25), and (26), we obtain

$$\sqrt{1 - D^2} \geq \Delta(\sigma_y W_0) \Delta(\sigma_z W_0) \geq |\langle \sigma_x \rangle| = V. \quad (27)$$

This directly yields the duality relation, Eq. (1). Alternatively, the commutator $[\sigma_x, (\sigma_y W_0)] = 2i\sigma_z W_0$ can be used to obtain the uncertainty relation

$$\sqrt{1 - V^2} \geq \Delta\sigma_x \Delta(\sigma_y W_0) \geq |\langle \sigma_z W_0 \rangle| = D, \quad (28)$$

which again yields the duality relation.

To summarize, we have demonstrated here that in an arbitrary which-way scheme, the duality relation can be expressed in the form of a Heisenberg–Robertson uncertainty relation for some suitably chosen observables.

IV. DISCUSSION

The above calculation reveals a new aspect of the connection between wave–particle duality and the uncertainty relation. We would like to add a few comments concerning the interpretation of this result.

Let us first point out that the uncertainty relation used in our calculation is not the position–momentum uncertainty relation. This is obvious, because, for example, the observables considered here have only two eigenvalues, namely ± 1 , whereas position and momentum have a continuous spectrum of eigenvalues.

Second, we note that for the case without a which-way marker, Eq. (2) is *equivalent* to the uncertainty relations for $\Delta\sigma_x \Delta\sigma_y$ and $\Delta\sigma_y \Delta\sigma_z$, Eqs. (12) and (13). This equivalence can be read in both directions: In one direction, as discussed above, the uncertainty relation implies Eq. (2). In the other direction, Eq. (2) implies the uncertainty relation for these specific observables.

Third, we would like to draw attention to the fact that the uncertainty relation for $\Delta\sigma_z \Delta\sigma_x$, Eq. (14), yields a trivial result. This is somewhat surprising, because from Eq. (10) we concluded that σ_x represents the wave character, whereas σ_z represents the particle character. Since we are investigating the limit for the simultaneous presence of wave character and particle character, one might have guessed that the uncertainty relation for $\Delta\sigma_z \Delta\sigma_x$ could yield this limit. However, this is not the case. Instead, $\Delta\sigma_y$ is employed in our calculation. An intuitive interpretation of σ_y in terms of a wave picture or a particle picture is not obvious.

Next, we would like to mention that the observables whose uncertainty relations we evaluate in Eqs. (12) and (13) depend on the density matrix, ρ . In the presentation in Sec. II, this fact is somewhat hidden in our choice of the relative phase of states $| + \rangle$ and $| - \rangle$, i.e., $\varphi_0 = 0$. The dependence on ρ becomes more obvious, if we consider arbitrary values of φ_0 . In this case, we can define the observables

$$\Sigma_x = \sigma_x \cos \varphi_0 - \sigma_y \sin \varphi_0, \quad (29)$$

$$\Sigma_y = \sigma_x \sin \varphi_0 + \sigma_y \cos \varphi_0, \quad (30)$$

$$\Sigma_z = \sigma_z, \quad (31)$$

which take the role of σ_x , σ_y , and σ_z in our above presentation. Obviously, these observables depend on ρ via φ_0 . As the commutation relations of the Σ 's and σ 's are the same, Eq. (2) can be derived analogously. The situation is similar in Sec. III.

Finally, we will discuss whether either correlations (i.e., entanglement) or uncertainty relations are more closely connected to wave–particle duality. For that purpose, we will investigate all the explanations for the loss of interference fringes, referenced in Sec. I. We will sort these explanations into three categories, depending on whether they employ

- (1) some uncertainty relation,
- (2) correlations,
- (3) correlations and some uncertainty relation.

The textbook explanations for Einstein's recoiling slit in Ref. 1 and Feynman's light microscope in Ref. 2 are based on the position–momentum uncertainty relation. The Scully–Englert–Walther explanation⁴ as well as the derivations of the duality relation in Refs. 12 and 13 are based on the correlations. Our derivation as well as the discussion of Wiseman *et al.*³ make use of both the correlations and some uncertainty relation. This is because these calculations involve the density matrix for the total system, consisting of the object plus the which-way marker. Consequently, the full quantum correlations between these subsystems are embodied in these formalisms.

The above categorization reveals a crucial point: The explanations for the loss of interference fringes involving *only* the uncertainty relation are (so far) limited to a few special schemes. In other words: There are several other schemes for which no such explanation is known, see, e.g., Refs. 4 and

11. In the language of Ref. 3, the loss of interference in these schemes cannot be explained in terms of “classical momentum transfer.” On the other hand, explanations involving *only* correlations apply to all which-way schemes known so far. This leads us to the conclusion that wave–particle duality is connected to correlations more closely than to the uncertainty relation.

^{a)}Electronic mail: gerhard.rempel@mpq.mpg.de

- ¹N. Bohr, “Discussion with Einstein on epistemological problems in atomic physics,” in *Albert Einstein: Philosopher-Scientist*, edited by P. A. Schilpp (Library of Living Philosophers, Evanston, 1949), pp. 200–241, reprinted in J. A. Wheeler and W. H. Zurek, *Quantum Theory and Measurement* (Princeton U.P., Princeton, 1983), pp. 9–49.
- ²R. P. Feynman, R. B. Leighton, and M. Sands, *The Feynman Lectures on Physics* (Addison-Wesley, Reading, MA, 1965), Vol. III, Chap. 1.
- ³H. M. Wiseman, F. E. Harrison, M. J. Collett, S. M. Tan, D. F. Walls, and R. B. Killip, “Nonlocal momentum transfer in welcher weg measurements,” *Phys. Rev. A* **56**, 55–75 (1997).
- ⁴M. O. Scully, B.-G. Englert, and H. Walther, “Quantum optical tests of complementarity,” *Nature (London)* **351**, 111–116 (1991).
- ⁵S. Haroche, “Quantum beats and time-resolved fluorescence spectroscopy”, in *High-resolution Laser Spectroscopy*, edited by K. Shimoda, Topics in Applied Physics Vol. 13 (Springer, New York, 1976), pp. 253–313.
- ⁶X. Y. Zou, L. J. Wang, and L. Mandel, “Induced coherence and indistinguishability in optical interference,” *Phys. Rev. Lett.* **67**, 318–321 (1991).
- ⁷T. J. Herzog, P. G. Kwiat, H. Weinfurter, and A. Zeilinger, “Complementarity and the quantum eraser,” *Phys. Rev. Lett.* **75**, 3034–3037 (1995).
- ⁸U. Eichmann, J. C. Bergquist, J. J. Bollinger, J. M. Gilliban, W. M. Itano, D. J. Wineland, and M. G. Raizen, “Young’s interference experiment with light scattered from two atoms,” *Phys. Rev. Lett.* **70**, 2359–2362 (1993).
- ⁹H. Rauch, A. Zeilinger, G. Badurek, A. Wilfing, W. Bauspiess, and U. Bonse, “Verification of coherent spinor rotation of fermions,” *Phys. Lett. A* **54**, 425–427 (1975).
- ¹⁰G. Badurek, H. Rauch, and D. Tuppinger, “Neutron interferometric double-resonance experiment,” *Phys. Rev. A* **34**, 2600–2608 (1986).
- ¹¹S. Dürr, T. Nonn, and G. Rempe, “Origin of quantum-mechanical complementarity probed by a ‘which-way’ experiment in an atom interferometer,” *Nature (London)* **395**, 33–37 (1998).
- ¹²G. Jaeger, A. Shimony, and L. Vaidman, “Two interferometric complementarities,” *Phys. Rev. A* **51**, 54–67 (1995).
- ¹³B.-G. Englert, “Fringe visibility and which-way information: An inequality,” *Phys. Rev. Lett.* **77**, 2154–2157 (1996).
- ¹⁴S. Dürr, T. Nonn, and G. Rempe, “Fringe visibility and which-way information in an atom interferometer,” *Phys. Rev. Lett.* **81**, 5705–5709 (1998).
- ¹⁵P. D. D. Schwindt, P. G. Kwiat, and B.-G. Englert, “Quantitative wave–particle duality and nonerasing quantum erasure,” *Phys. Rev. A* **60**, 4285–4290 (1999).
- ¹⁶W. K. Wootters and W. H. Zurek, “Complementarity in the double-slit experiment: Quantum nonseparability and a quantitative statement of Bohr’s principle,” *Phys. Rev. D* **19**, 473–484 (1979).
- ¹⁷L. S. Bartell, “Complementarity in the double-slit experiment: On simple realizable systems for observing intermediate particle–wave behavior,” *Phys. Rev. D* **21**, 1698–1699 (1980).
- ¹⁸R. J. Glauber, “Amplifiers, attenuators, and Schrödinger’s cat,” *Ann. (N.Y.) Acad. Sci.* **480**, 336–372 (1986).
- ¹⁹D. M. Greenberger and A. Yasin, “Simultaneous wave and particle knowledge in a neutron interferometer,” *Phys. Lett. A* **128**, 391–394 (1988).
- ²⁰L. Mandel, “Coherence and indistinguishability,” *Opt. Lett.* **16**, 1882–1883 (1991).
- ²¹J. Summhammer, H. Rauch, and D. Tuppinger, “Stochastic and deterministic absorption in neutron-interference experiments,” *Phys. Rev. A* **36**, 4447–4455 (1987).
- ²²P. Mittelstaedt, A. Prieur, and R. Schieder, “Unsharp particle–wave duality in a photon split-beam experiment,” *Found. Phys.* **17**, 891–903 (1987).
- ²³W. Heisenberg, “Über den anschaulichen Inhalt der quantentheoretischen Kinematik und Mechanik,” *Z. Phys.* **43**, 172–198 (1927); for an English translation see J. A. Wheeler and W. H. Zurek in Ref. 1, pp. 62–84.
- ²⁴H. P. Robertson, “The uncertainty principle,” *Phys. Rev.* **34**, 163–164 (1929).
- ²⁵W. H. Zurek, “Decoherence and the transition from quantum to classical,” *Phys. Today* **44**, 36–44 (October 1991).
- ²⁶B.-G. Englert, “Remarks on some basic issues in quantum mechanics,” *Z. Naturforsch., A: Phys. Sci.* **54**, 11–32 (1999).

Vacuum-Stimulated Raman Scattering Based on Adiabatic Passage in a High-Finesse Optical Cavity

M. Hennrich, T. Legero, A. Kuhn, and G. Rempe

Max-Planck-Institut für Quantenoptik, Hans-Kopfermann-Strasse 1, D-85748 Garching, Germany
(Received 21 August 2000)

We report on the first observation of stimulated Raman scattering from a Λ -type three-level atom, where the stimulation is realized by the vacuum field of a high-finesse optical cavity. The scheme produces one intracavity photon by means of an adiabatic passage technique based on a counterintuitive interaction sequence between pump laser and cavity field. This photon leaves the cavity through the less-reflecting mirror. The emission rate shows a characteristic dependence on the cavity and pump detuning, and the observed spectra have a subnatural linewidth. The results are in excellent agreement with numerical simulations.

PACS numbers: 32.80.Qk, 03.67.-a, 42.50.Ct, 42.65.Dr

In the past few years, interesting proposals on the generation of nonclassical states of light in optical cavities [1,2] and on the controlled generation of single photons from such cavities [3,4] were made. All of these schemes are based on a technique known as STIRAP (stimulated Raman scattering involving adiabatic passage) [5,6] or a variant thereof, and incorporate the time dependent interaction of an atom with the field mode of an optical cavity. The operation principle is related to that of a Raman laser [7], with the difference that now a single atom interacts with an empty cavity mode. Other schemes for the preparation of Fock states are based on vacuum Rabi oscillations or, more generally, π pulses in a two-level atom. In these cases, the need for a long-lived excited atomic state restricts experiments to the microwave regime [8,9], where the photon remains stored in a high- Q cavity.

Here, we report on the experimental realization of an excitation scheme that allows one to emit a visible photon into a well-defined mode of an empty cavity. This photon then leaves the cavity in a known direction. Our method is based on the single-photon generation scheme discussed in [4]. It relies on STIRAP [5,6], but, instead of using two delayed laser pulses, we have only one exciting pump laser, combined with a strong coupling of a single atom to a single cavity mode [10,11]. This strong coupling induces the anti-Stokes transition of the Raman process.

Figure 1 depicts the excitation scheme for the ^{85}Rb -atoms used in our experiment. A Λ -type three-level scheme is realized by the two $5S_{1/2}$ hyperfine ground states $F = 3$ and $F = 2$, which we label $|u\rangle$ and $|g\rangle$, respectively. The $F = 3$ hyperfine level of the electronically excited state, $5P_{3/2}$, forms the intermediate state, $|e\rangle$. The atom interacts with a single-mode of an optical cavity, with states $|0\rangle$ and $|1\rangle$ denoting zero and one photon in the mode, respectively. The cavity resonance frequency, ω_C , is close to the atomic transition frequency between states $|e\rangle$ and $|g\rangle$, but far off resonance from the $|e\rangle$ to $|u\rangle$ transition. Hence, only the product states $|e, 0\rangle$ and $|g, 1\rangle$ are coupled by the cavity. For this transition, the vacuum

Rabi frequency,

$$2g(t) = 2g_0 \exp\left[-\left(\frac{tv}{w_C}\right)^2\right], \quad (1)$$

is time dependent since the atom moves with velocity v across the waist w_C of the Gaussian cavity mode. Its peak amplitude is given by the atom-cavity coupling coefficient at an antinode, g_0 .

In addition to the interaction with the cavity mode, the atom is exposed to a pump laser beam which crosses the cavity axis at right angle. This beam is placed slightly downstream in the path of the atoms (by δ_x with respect to the cavity axis) and has a waist w_P , therefore causing a time dependent Rabi frequency

$$\Omega_P(t) = \Omega_0 \exp\left[-\left(\frac{tv - \delta_x}{w_P}\right)^2\right]. \quad (2)$$

The pump frequency is near resonant with the transition between $|u, 0\rangle$ and $|e, 0\rangle$, thereby coupling these states.

In a frame rotating with the cavity frequency and the pump laser frequency, the Hamiltonian is given by

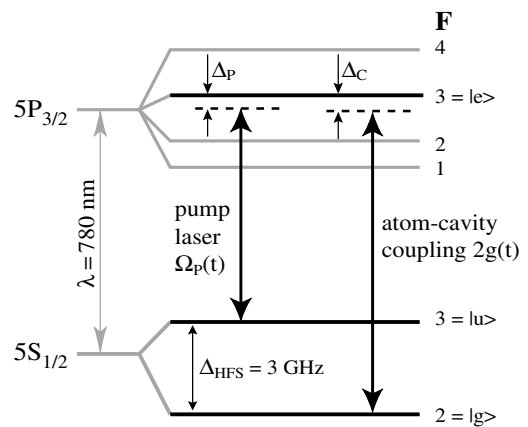


FIG. 1. Scheme of the relevant levels, transitions, and detunings of the ^{85}Rb atom coupled to the pump laser and the cavity.

$$\begin{aligned}
 H(t) = & \hbar[\Delta_P|u\rangle\langle u| + \Delta_C|g\rangle\langle g| \\
 & + g(t)(|e\rangle\langle g|a + a^\dagger|g\rangle\langle e|) \\
 & + \frac{1}{2}\Omega_P(t)(|e\rangle\langle u| + |u\rangle\langle e|)]. \quad (3)
 \end{aligned}$$

Here, Δ_C and Δ_P denote the detunings of the cavity and the pump beam from their respective atomic resonances, and a and a^\dagger are the annihilation and creation operators of the cavity field. The pump beam is treated semiclassically. On Raman resonance, i.e., for $\Delta_C = \Delta_P$, one of the eigenstates of this interaction Hamiltonian reads

$$|a^0(t)\rangle = \frac{2g(t)|u, 0\rangle - \Omega_P(t)|g, 1\rangle}{\sqrt{4g^2(t) + \Omega_P^2(t)}}. \quad (4)$$

This is a dark state without any contribution from the electronically excited level $|e, 0\rangle$. Therefore losses due to spontaneous emission cannot occur, provided the state vector of the system, $|\Psi\rangle$, follows $|a^0\rangle$ throughout the Raman excitation.

The atom is prepared in state $|u\rangle$ before it enters the empty cavity, i.e., atom and field start in state $|u, 0\rangle$. Since the pump beam is displaced by δ_x with respect to the cavity axis, the atom is subject to a counterintuitive delayed pulse sequence, i.e., due to the initial condition $2g \gg \Omega_P$, the evolution starts with $\langle\Psi|a^0\rangle = 1$. The subsequent interaction with the pump beam leads to $\Omega_P \gg 2g$, which implies the evolution of $|a^0\rangle$ into state $|g, 1\rangle$. Provided the state vector $|\Psi\rangle$ is able to follow, the system is transferred to $|g, 1\rangle$, and a photon is placed in the cavity mode. Since this photon is emitted with the cavity energy decay rate, 2κ , the empty cavity state, $|g, 0\rangle$, is finally reached and the atom-cavity system decouples from any further interaction.

This simple excitation scheme relies on three conditions. First, the detunings of the cavity, Δ_C , and of the pump pulse, Δ_P , must allow a Raman transition, i.e.,

$$|\Delta_C - \Delta_P| < 2\kappa. \quad (5)$$

Second, the condition for $|\Psi\rangle$ adiabatically following $|a^0\rangle$ must be met [4,5],

$$(2g_0w_C/v, \Omega_0w_P/v) \gg 1. \quad (6)$$

Third, either the interaction time must be significantly longer than $(2\kappa)^{-1}$ to allow the emission of the photon before it is reabsorbed by the atom due to coherent population return [4,6] or, alternatively, the interaction with the pump beam must be strong when the atom leaves the cavity to avoid this reverse process.

A numerical simulation for a single atom crossing the cavity is shown in Fig. 2. To include the cavity-field decay rate, κ , and the spontaneous emission rate of the atom, Γ , we have employed the density-matrix formalism described in [4]. For the resonant situation, $\Delta_P = \Delta_C = 0$, shown here, the total emission probability, P_{emit} , is expected to reach 90%. For the considered waists and amplitudes, Fig. 2(c) shows that P_{emit} reaches its maximum for $\delta_x/v = 45 \mu\text{s}$. Note also that P_{emit} is vanishingly small if

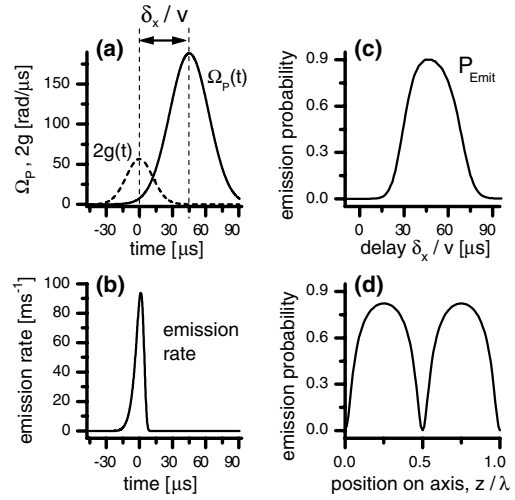


FIG. 2. Simulation of a resonant atom-cavity interaction sequence for a cavity decay constant, $2\kappa = 2\pi \times 2.5$ MHz, an atomic decay constant of $\Gamma = 2\pi \times 6$ MHz, and atoms traveling at $v = 2$ m/s. (a) $\Omega_P(t)$ and $2g(t)$ shown for experimental amplitudes and waists, $w_C = 35 \mu\text{m}$ and $w_P = 50 \mu\text{m}$. (b) Photon emission rate for a delay of $\delta_x/v = 45 \mu\text{s}$. The integral of the rate yields a total photon emission probability, P_{emit} , of 90%. (c) P_{emit} as a function of the delay, δ_x/v , between cavity and pump interaction. (d) P_{emit} as a function of the atomic position on the cavity axis for a delay of $\delta_x/v = 35 \mu\text{s}$.

the interaction with the pump beam coincides or precedes the interaction with the cavity mode. Figure 2(d) shows P_{emit} as a function of the atom's position on the cavity axis for the delay realized in the experiment. Because of the standing wave mode structure, the emission probability is zero at the nodes, and shows maxima at the antinodes. Since the dependence of P_{emit} on the position dependent coupling constant, g , is highly nonlinear and saturates for large g , the gaps around the nodes are much narrower than the plateaus surrounding the antinodes.

Figure 3 depicts the case where $\Delta_P \neq \Delta_C$. It is obvious that P_{emit} is close to unity if the excitation is Raman resonant ($\Delta_P = \Delta_C$). However, for the delay $\delta_x/v = 35 \mu\text{s}$ chosen here, a smaller signal is expected for $\Delta_P = \Delta_C = 0$, since the waist of the pump, w_P , is larger than w_C , and resonant excitation of the atom prior to the interaction with the cavity mode cannot be neglected.

To realize the proposed scheme, we have chosen the setup sketched in Fig. 4. A cloud of ^{85}Rb atoms is prepared in the $5S_{1/2}, F = 3$ state and released from a magneto-optical trap (MOT) at a temperature of $\approx 10 \mu\text{K}$. A small fraction (up to 100 atoms) falls through a stack of apertures and enters the mode volume of an optical cavity at a speed of 2 m/s. The cavity is composed of two mirrors with a curvature of 50 mm and a distance of 1 mm. The waist of the TEM_{00} mode is $w_C = 35 \mu\text{m}$, and in the antinodes the coupling coefficient is $g_0 = 2\pi \times 4.5$ MHz. The finesse of 61 000 corresponds to a linewidth $2\kappa = 2\pi \times 2.5$ MHz (FWHM), which is significantly smaller than the

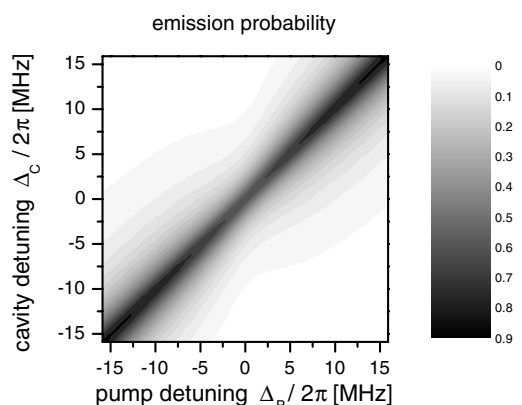


FIG. 3. Photon emission probability as a function of cavity and pump detuning, calculated for a pulse delay of $\delta_x/v = 35 \mu\text{s}$ and the parameters of Fig. 2. The chosen delay gives the best fit with the experimental data shown in Fig. 5.

natural linewidth of the ^{85}Rb atoms. While one cavity mirror is highly reflective ($1 - R = 4 \times 10^{-6}$), the transmission of the other is $25\times$ higher to emit the photons in one direction only. A single-photon counting module (SPCM) with a quantum efficiency of 50% is used to detect them.

A reference laser is used to stabilize the cavity close to resonance with the $5S_{1/2}, F = 2 \leftrightarrow 5P_{3/2}, F = 3$ transition with a lock-in technique. However, since an empty cavity is needed for the experiment, this laser is blocked 3.7 ms before the atoms enter the cavity.

The pump beam is close to resonance with the $5S_{1/2}, F = 3 \leftrightarrow 5P_{3/2}, F = 3$ transition and crosses the cavity transverse to its axis. This laser is focused to a waist of $50 \mu\text{m}$ and has a power of $5.5 \mu\text{W}$, which corresponds to a peak Rabi frequency $\Omega_0 = 2\pi \times 30 \text{ MHz}$.

The desired counterintuitive pulse sequence for STIRAP is realized by time of flight. The atoms first enter the cavity mode and therefore experience a strong coupling on the anti-Stokes transition, whereas the interaction with the pump beam is delayed, since it crosses the cavity mode slightly downstream. This delay has been optimized to achieve a high flux of photons leaving the cavity.

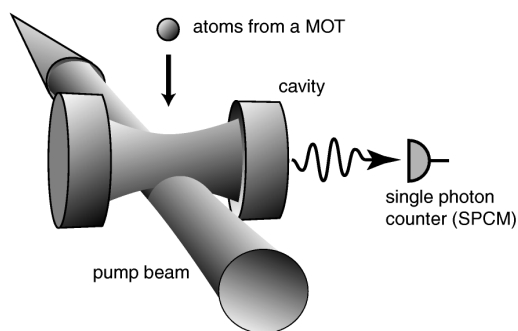


FIG. 4. Sketch of the experimental setup. The pump beam is displaced with respect to the cavity mode.

4874

Figure 5(a) shows the number of counted photons emerging from the cavity as a function of the pump pulse detuning, Δ_p , in case of a resonant cavity, $\Delta_c = 0$. The detunings of the cavity and the pump laser are both adjusted by means of acousto-optic modulators. To register the data, the MOT has been loaded and dropped across the cavity 50 times. The atom cloud needs 6.5 ms (FWHM) to cross the cavity mode, and, within this interval, the photons emerging from the cavity are measured by the SPCM and recorded by a transient digitizer during 2.6 ms with a time resolution of 25 MHz. Therefore, the signal is observed for a total time of 130 ms. Because of the dark count rate of 390 Hz of the SPCM, the total number of dark counts in the interval is limited to 51 ± 7 .

In the resonant case, one expects a small probability for atomic excitation. This could lead to a small but cavity enhanced spontaneous emission into the cavity mode, as has been shown previously [12]. Our numerical simulation shows that an excited atom at the antinode emits into the resonant cavity mode with a probability that can be as high as 26%, indicating that even in this case most of the spontaneously emitted photons are lost in a random direction. This loss explains the smaller peak emission rate with respect to the off-resonant cases discussed below. Note that the cavity mode covers only a small solid angle of $\approx 4\pi \times 2.6 \times 10^{-5} \text{ sr}$, therefore

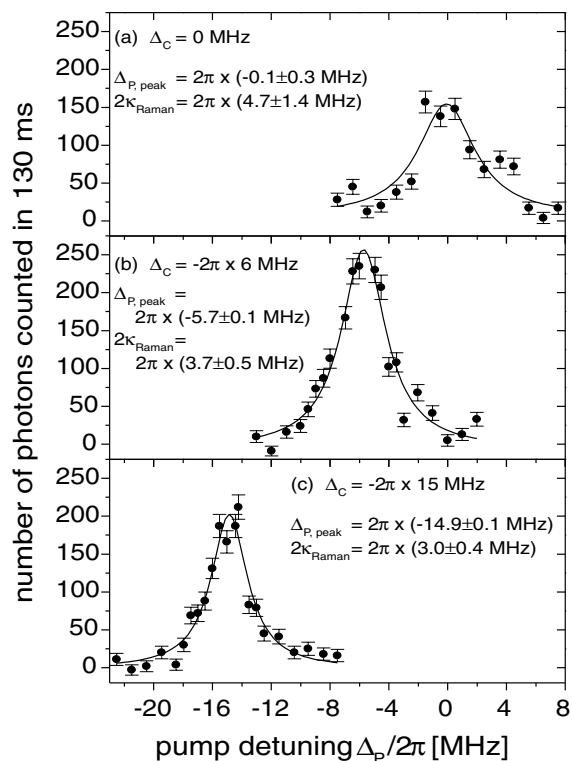


FIG. 5. Number of photons from the cavity as a function of the pump laser detuning, Δ_p , for three different cavity detunings. The solid lines are Lorentzian fits to the data.

the calculated spontaneous emission rate into the cavity is enhanced by a factor of 10^4 . However, the linewidth is subnatural, and therefore the observed signal cannot be attributed to an excitation by the pump beam followed by enhanced spontaneous emission.

This is even more evident if the cavity is detuned [Figs. 5(b) and 5(c)]. The emission peak is pulled away from the atomic resonance following the Raman resonance condition, $\Delta_P = \Delta_C$. Such a displacement proves that the light emission is not the result of a pump transition followed by enhanced spontaneous emission into the cavity. Moreover, Δ_P is too high for an electronic excitation of the atoms. Therefore, the far out-reaching wings of the pump beam no longer excite the atoms prior to their interaction with the cavity mode. The losses vanish, and the peak photon emission probability is higher than for the resonant case. Note also that the observed linewidth is much smaller than the natural linewidth, $\Gamma = 2\pi \times 6$ MHz, of the atom. For $\Delta_C = -2\pi \times 15$ MHz, the line is only 3 MHz wide and approaches the linewidth $2\kappa = 2\pi \times 2.5$ MHz of the cavity, which also limits the width of the Raman transition, since 2κ is the decay rate of the final state, $|g, 1\rangle$.

In our discussion, we have assumed that the atoms interact with the cavity one-by-one. This is justified according to the following estimation: A mechanical slit restricts the atom's maximum distance from the cavity axis to ± 50 μm . The spatial variation of g along [Fig. 2(d)] and perpendicular to the cavity axis reduces the average emission probability to 37% per atom crossing the slit and the pump beam. Because of the low quantum efficiency of the SPCM and unavoidable cavity losses, only about 40% of the generated photons are detected. Therefore the maximum measured rate of 230 events/130 ms corresponds to a generation rate of 4.4 photons/ms, and at least 12 atoms/ms are needed to explain this signal. Since the photon generation takes 12 μs [FWHM, Fig. 2(b)], the probability that a second atom interacts with the cavity simultaneously is 14%. This is small and, hence, negligible.

All observed features are in excellent agreement with our simulation, and we therefore conclude that the photon emission is caused by a vacuum-stimulated Raman transition, i.e., the coupling to the cavity, $g(t)$, and the Rabi frequency of the pump laser, $\Omega_P(t)$, are both high enough to ensure an adiabatic evolution of the system, thus forcing the state vector $|\Psi\rangle$ to follow the dark state $|a^0\rangle$ throughout the interaction. Loss due to spontaneous emission is suppressed, and the photons are emitted into a single mode of the radiation field with well-determined frequency and direction.

The scheme can be used to generate single, well-characterized photons on demand, provided the Raman excitation is performed in a controlled, triggered way. In contrast to other single-photon sources [13], these photons will have a narrow bandwidth and a directed

emission. Finally, we state that the photon generation process depends on the initial state of the atom interacting with the cavity. If the atom is prepared in a superposition of states $|g, 0\rangle$ and $|u, 0\rangle$, prior to the interaction, this state will be mapped onto the emitted photon. A second atom placed in another cavity could act as a receiver, and, with the suitable pump pulse sequence applied to the emitting and the receiving atom, a quantum teleportation of the atom's internal state could be realized [14].

This work was partially supported by the focused research program, "Quantum Information Processing," of the Deutsche Forschungsgemeinschaft and the QUBITS project of the IST program of the European Union.

-
- [1] A.S. Parkins, P. Marte, P. Zoller, and H.J. Kimble, *Phys. Rev. Lett.* **71**, 3095 (1993); A.S. Parkins, P. Marte, P. Zoller, O. Carnal, and H.J. Kimble, *Phys. Rev. A* **51**, 1578 (1995).
 - [2] W. Lange and H.J. Kimble, *Phys. Rev. A* **61**, 63817 (2000).
 - [3] C.K. Law and J.H. Eberly, *Phys. Rev. Lett.* **76**, 1055 (1996); C.K. Law and H.J. Kimble, *J. Mod. Opt.* **44**, 2067 (1997).
 - [4] A. Kuhn, M. Hennrich, T. Bundo, and G. Rempe, *Appl. Phys. B* **69**, 373 (1999).
 - [5] For a review, see K. Bergmann and B.W. Shore in *Molecular Dynamics and Stimulated Emission Pumping*, edited by H.L. Dai and R.W. Field (World Scientific, Singapore, 1995), p. 315–373.
 - [6] A. Kuhn, S. Steuerwald, and K. Bergmann, *Eur. Phys. J. D* **1**, 57 (1998).
 - [7] M. Becker, U. Gaubatz, K. Bergmann, and P.L. Jones, *J. Chem. Phys.* **87**, 5064 (1987).
 - [8] G. Nogues, A. Rauschenbeutel, S. Osnaghi, M. Brune, J.M. Raimond, and S. Haroche, *Nature (London)* **400**, 239 (1999).
 - [9] B.T.H. Varcoe, S. Brattke, M. Weidinger, and H. Walther, *Nature (London)* **403**, 743 (2000).
 - [10] H. Mabuchi, Q.A. Turchette, M.S. Chapman, and H.J. Kimble, *Opt. Lett.* **21**, 1393 (1996).
 - [11] P. Münstermann, T. Fischer, P.W.H. Pinkse, and G. Rempe, *Opt. Commun.* **159**, 63 (1999).
 - [12] D.J. Heinzen, J.J. Childs, J.E. Thomas, and M.S. Feld, *Phys. Rev. Lett.* **58**, 1320 (1987); D.J. Heinzen and M.S. Feld, *Phys. Rev. Lett.* **59**, 2623 (1987).
 - [13] J. Kim, O. Benson, H. Kan, and Y. Yamamoto, *Nature (London)* **397**, 500 (1999); C. Brunel, B. Lounis, P. Tamarat, and M. Orrit, *Phys. Rev. Lett.* **83**, 2722 (1999); C. Kurtsiefer, S. Mayer, P. Zarda, and H. Weinfurter, *Phys. Rev. Lett.* **85**, 290 (2000); R. Brouri, A. Beveratos, J.-P. Poizat, and P. Grangier, *Opt. Lett.* **25**, 1294 (2000); P. Michler, A. Imamoğlu, M.D. Mason, P.J. Carson, G.F. Strouse, and S.K. Buratto, *Nature (London)* **406**, 968 (2000).
 - [14] J.I. Cirac, P. Zoller, H.J. Kimble, and H. Mabuchi, *Phys. Rev. Lett.* **78**, 3221 (1997).

Avalanches in a Bose-Einstein Condensate

J. Schuster, A. Marte, S. Amthar, B. Sang, and G. Rempe

Max-Planck-Institut für Quantenoptik, Hans-Kopfermann-Strasse 1, D-85748 Garching, Germany

H. C. W. Beijerinck

Physics Department, Eindhoven University of Technology, P.O. Box 513, 5600 MB Eindhoven, The Netherlands
(Received 28 November 2000; revised manuscript received 16 April 2001; published 8 October 2001)

Collisional avalanches are identified to be responsible for an 8-fold increase of the initial loss rate of a large ^{87}Rb condensate. We show that the collisional opacity of an ultracold gas exhibits a critical value. When exceeded, losses due to inelastic collisions are substantially enhanced. Under these circumstances, reaching the hydrodynamic regime in conventional Bose-Einstein condensation experiments is highly questionable.

DOI: 10.1103/PhysRevLett.87.170404

PACS numbers: 03.75.Fi, 32.80.Pj, 34.50.-s, 82.20.Pm

One of the current goals in the field of Bose-Einstein condensation (BEC) is the production of a condensate in the collisionally opaque or hydrodynamic regime, where the mean free path of an atom is much less than the size of the sample. This would offer the opportunity to study striking phenomena such as quantum depletion or dynamical local thermal equilibrium. In this context, one possible approach is to increase the interaction among the atoms by means of Feshbach resonances [1]. It has been observed, however, that in their vicinity the large cross section for elastic collisions is accompanied by a dramatic increase of atom losses [2,3]. Hence, it seems advantageous to follow a different route by producing large and dense condensates.

In this Letter, we conclude that the collisionally opaque regime can hardly be reached in alkali BEC experiments. We identify an intrinsic decay process that severely limits the average column density $\langle nl \rangle$ of condensates at values achieved in present BEC experiments. It is based on collisional avalanches that are triggered by inelastic collisions between condensate atoms. A considerable part of the energy released in these initiatory collisions is distributed among trapped atoms resulting in a dramatic enhancement of the total loss from the condensate. In analogy to the critical mass needed for a nuclear explosion, we define a critical value of the collisional opacity $\langle nl \rangle \sigma_s$, with $\sigma_s = 8\pi a^2$ the s -wave cross section for like atoms and a the scattering length. The *critical opacity* equals 0.693, corresponding to a collision probability of 0.5. Related scenarios have been discussed in Refs. [4,5], but were assumed to play a minor role in the experimentally relevant region. However, we present strong experimental evidence that the anomalous decay of our ^{87}Rb condensate is caused by collisional avalanches. This is supported by the good agreement of a simple model with the data.

The crucial point for the occurrence of an avalanche is whether the products of a one-, two-, or three-body decay process have a substantial probability

$$p(E) = 1 - \exp[-\langle nl \rangle \sigma(E)] \quad (1)$$

of undergoing secondary collisions before leaving the trap [6], with $\sigma(E)$ the total cross section at kinetic energy E . The collision probability varies significantly with temperature and is usually highest in the s -wave scattering regime.

Here, the differential cross section is isotropic in the center-of-mass system; in the laboratory system the two atoms fly apart at an angle of $\pi/2$ on average. The energy of the projectile is on average equally distributed among the two colliding atoms. This implies that each collision results in *two* new atoms that both can continue their collisional havoc in the trap until they leave the condensate (Fig. 1). If the probability for collisions is higher than 0.5, the average number of colliding atoms increases with every step of the collisional chain which now becomes self-sustaining.

To calculate the total loss from the condensate, we start from the well-known loss rates $\dot{N}_i = -K_i N \langle n^{i-1} \rangle$, with $i = 1, 2, 3$ associated with one-, two-, and three-body decay processes with rate constant K_i , respectively. Here, N is the number of atoms in the gas with the density distribution $n(\vec{r})$. Depending on the energy of the decay products, typically a few or even no further collisions are needed to generate an atom with an energy $E_{i,s}$ whose next collision

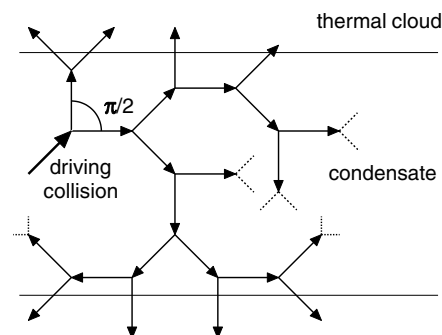


FIG. 1. Sketch of a collisional avalanche in a homogeneous condensate with a radius equal to twice the mean free path $(n\sigma_s)^{-1}$, illustrating the enhancement of the loss rate.

would be in the s -wave regime. The probability for this collisional chain is $p_{i,1} \cdot p_{i,2} \cdots = \tilde{p}_i$ with $p_{i,n} = p(E_{i,n})$. During this process, on average \tilde{g}_i atoms are lost from the condensate without undergoing secondary collisions. Next, an atom with energy $E_{i,s}$ induces an avalanche with a collision probability $p_s = 1 - \exp[-\langle nl \rangle \sigma_s]$ that now is independent of energy. Consequently, atoms with an energy $E_{i,s}/2^k$ in the k th step of an avalanche are generated with a probability of $\tilde{p}_i p_s^k$. Since every collision now results in two projectiles in the next step, the degeneracy of step k is 2^k . The rate at which atoms are lost from this avalanche step is $\tilde{p}_i \dot{N}_i 2^k p_s^k (1 - p_s)$ and the total loss rate from the condensate becomes

$$\dot{N}_{i,\text{aval}} = \dot{N}_i \left[\tilde{g}_i + \tilde{p}_i (1 - p_s) \sum_{k=0}^{k_i^{\text{max}}} 2^k p_s^k \right], \quad (2)$$

where the sum extends over all relevant avalanche steps.

To determine the cutoff k_i^{max} , note that avalanche-enhanced losses can occur up to a step with an energy on the order of the chemical potential. However, when the energy falls short of the trap depth, E_{trap} , the atoms lost from the cold sample are still trapped. They will repeatedly penetrate the cloud and thus give rise to heating. This will either be compensated by an evaporation of atoms from the trap or will reduce the condensed fraction by increasing the temperature. Both possibilities are not described by Eq. (2). Therefore, we use $k_i^{\text{max}} \leq \log_2(E_{i,s}/E_{\text{trap}})$ as a cutoff and, hence, account only for immediate trap losses.

The additional heat-induced depletion caused by trapped avalanche atoms can easily be estimated for the case that the temperature is fixed by the trap depth. Each atom participating in step $(k_i^{\text{max}} + 1)$ of the avalanche will finally dump about the energy $E_{\text{trap}}/2$ into the system. Since any evaporated atom takes the energy E_{trap} with it, about half as many atoms as are produced in the step $(k_i^{\text{max}} + 1)$ of the avalanche have to be evaporated to keep the temperature constant. Hence, the evaporation rate is

$$\dot{N}_{i,\text{heat}} \approx (1/2) \tilde{p}_i \dot{N}_i 2^{(k_i^{\text{max}} + 1)} p_s^{(k_i^{\text{max}} + 1)}. \quad (3)$$

Equation (2) predicts substantially enhanced losses as soon as the critical opacity is exceeded. However, for a given k_i^{max} there is a second critical value of the opacity above which the loss rate $\dot{N}_{i,\text{aval}}$ decreases again. Now, with increasing opacity the limited trap depth continuously loses its shielding effect against the products of inelastic collisions, since most avalanches generate trapped particles. In the collisional regime with $p_s \approx 1$, the energy released in an inelastic process will be entirely dissipated in the system. This results in an explosionlike particle loss according to Eq. (3).

To apply our model, the column density must be evaluated according to

$$\langle nl \rangle = \int [n(\vec{r})/N] \int [n(\vec{r} + \vec{R})/4\pi R^2] d^3R d^3r \quad (4)$$

$$= cn_p W_{\perp} \int_0^{\infty} dx (1 + x^2)^{-1} (1 + \varepsilon^2 x^2)^{-1/2}, \quad (5)$$

where the second line is the result for the case of a harmonic potential with cylindrical symmetry. Here, $\varepsilon = \omega_{\parallel}/\omega_{\perp}$ is the ratio of the trap frequencies and n_p is the peak density of the cold sample. For the parabolic density distribution of the condensate, W_{\perp} is the half radial width and $c = 5/12$. Because of the scaling $n_p \propto N^{2/5}$ and $W_{\perp} \propto N^{1/5}$ the column density of a condensate scales as $N^{3/5}$, so that the effect of multiple collisions is quite persistent. For a Gaussian distribution we find $W_{\perp} = \sigma_{\perp}$, $c = \sqrt{\pi}/8$, and a scaling according to $\langle nl \rangle \propto N$. In a harmonic potential, the ideal Bose distribution can be represented as a sum of Gaussian distributions and the latter result can thus be used to evaluate the column density close to degeneracy. For a Bose distribution, the opacity scales disproportionate to N , resulting in a faster decline of the avalanche enhancement than in the case of a Thomas-Fermi distribution.

The next step is to identify the energies of the initial decay products. For a background gas collision, $E_{1,1}$ depends on the mass of the impinging particle that is assumed to be Rb in our system. In the case of spin relaxation, $E_{2,1}$ equals either the Zeeman energy or the hyperfine splitting energy. For three-body recombination $E_{3,1}$ has to be derived from the binding energy of the most weakly bound level in which the dimer is predominantly formed. Clearly, the molecule is likely to be deactivated in a subsequent inelastic collision with a condensate atom [7,8]. Deactivating collisions will be a serious problem in highly opaque clouds where atoms with higher energies still have high collision probabilities. In our experiment, however, the collision probability is significantly smaller at typical deactivation energies of 0.1 K than at the binding energy of the molecules in the last bound level. In our analysis we therefore do not account for avalanches triggered by deactivating collisions. The values of all parameters used to calculate the effective losses are listed in Table I. Note that in order to account for the avalanches triggered by the two-body decay, the partial rates associated with the various exit channels are needed since they correspond to different energies released in the process.

Finally, the presence of a diffuse atom cloud in the trapping volume can cause additional losses (see, e.g., [4]). In a steep magnetic trap with a depth of a few mK, such an ‘‘Oort’’ cloud is mainly a consequence of incomplete evaporation at high magnetic fields [9] or low radio frequency (rf) power. In our experiment, the temperature of the diffuse cloud will probably be on the order of 400 μ K, corresponding to the measured initial temperature of the magnetically trapped cloud. Even in a rf-shielded trap these atoms will penetrate the condensate giving rise to an additional decay rate according to $1/\tau = n_{\text{Oort}} \sigma_s v_{\text{Oort}}$, with n_{Oort} and v_{Oort} the density and the thermal velocity of the penetrating atoms, respectively. Collisions with Oort atoms will also trigger avalanches, because the collision energy is close to the s -wave regime.

To compare our data with the predictions of the model, the differential and the total scattering cross sections are

TABLE I. Rate constants for the initiatory processes and energies of the subsequent collisions that are necessary to generate the first avalanche atom with energy E_s .

i	Type	Rate constant K_i	$\Delta E_1, \dots, \Delta E_n = E_s$ [$(3/2)k_B$]
1	Background	$1/(39 \text{ s})^a$	4 K, 100, 5, 0.5 mK
2	Zeeman ^b	$1.4 \times 10^{-18} \text{ cm}^3/\text{s}$	0.022 mK
	$2 \times$ Zeeman ^c	$3.7 \times 10^{-17} \text{ cm}^3/\text{s}$	0.045 mK
	Hyperfine ^d	$2.2 \times 10^{-16} \text{ cm}^3/\text{s}$	109, 5, 0.5 mK
	$2 \times$ Hyperfine ^e	$1.3 \times 10^{-16} \text{ cm}^3/\text{s}$	219, 8, 0.5 mK
3	Recombination ^f	$1.8 \times 10^{-29} \text{ cm}^6/\text{s}$	0.54 mK ^g

^a[17]; ^{b,c,d,e}[11,18]; ^f[15,19]; ^g[20].

needed. Above a kinetic energy E/k_B of 60 mK we calculate the energy transfer by collisions using a model function for the small-angle differential cross section [10]. For collisions below 60 mK we use the numerical results from a full quantum treatment [11]. For ^{87}Rb in the $|2, 2\rangle$ state, the large contribution of a d -wave scattering resonance to the total cross section leads to $\sigma(E) \approx 4 \times \sigma_s$ at an energy of $E/k_B = 580 \mu\text{K}$ in the lab system. This almost coincides with the energy transferred to the third atom in a recombination event (Table I). Hence, a secondary collision of this atom will occur with a probability of 0.99 already when the probability for s -wave collisions among condensate atoms is 0.7. For kinetic energies $E/k_B \leq 1.5 \text{ mK}$, the total cross section obeys $\sigma(E) \approx \sigma_s$. For simplicity, we use σ_s for calculating avalanches in this energy range. Our model therefore yields a lower bound for the total loss.

The apparatus used to study the condensates has been described previously [12,13]. The experiment is performed with ^{87}Rb atoms in the $|2, 2\rangle$ state. A Ioffe-Pritchard magnetic trap with a bias field of 2 G and oscillation frequencies of $\omega_{\perp}/2\pi = 227 \text{ Hz}$ and $\omega_{\parallel}/2\pi = 24.5 \text{ Hz}$ is used. The atoms are cooled by rf evaporation and then held in the trap for a variable time interval. During the storage time, the trap depth is set to $E_{\text{trap}}/k_B = 4.4 \mu\text{K}$ by means of the rf shield. From the width of the density distribution after expansion the atom number N_C in the condensate is determined. At minimum storage time, we find $N_C = 1.1 \times 10^6$ atoms and $n_p = 6.4 \times 10^{14} \text{ cm}^{-3}$ and no discernible noncondensed fraction.

The decay curve of the condensate is shown in Fig. 2, revealing that about half the initial number of atoms is lost within the first 100 ms. The dotted line shows the theoretical prediction assuming that losses occur solely due to background gas collisions, spin relaxation and recombination (Table I). The observed loss is 8 times faster than predicted. Moreover, the additional decay is clearly non-exponential and can therefore not result from primary collisions with Oort atoms. Hence, multiple collisions have to be taken into account.

Indeed, with $\langle nl \rangle \sigma_s = 1.4$ the critical opacity is considerably exceeded. To the best of our knowledge, the corresponding s -wave collision probability of $p_s = 0.76$

has not been reached in published work on Rb condensates in the off-resonant scattering regime. This explains why our observations differ from those made in other experiments [14–16]. The dashed line displayed in Fig. 2 has been obtained by numerically integrating the rate equation $\dot{N} = \sum_{i=1}^3 (\mathcal{N}_{i,\text{aval}} + \mathcal{N}_{i,\text{heat}})$ that describes avalanche-enhanced losses according to Eqs. (2) and (3), without any adjustable parameter and neglecting the contribution of an Oort cloud. We find good agreement between theory and experiment within the first 200 ms, showing that collisional avalanches triggered by recombination events are responsible for the fast initial decay.

To investigate the role of an Oort cloud, we have performed a similar experiment with an atom cloud at a lower density. Figure 2 shows the decay of a noncondensed cloud with 1×10^7 atoms at a temperature of $1 \mu\text{K}$ and a peak density of $3.5 \times 10^{14} \text{ cm}^{-3}$. The number of atoms is determined from the total absorption of near-resonant laser light. The trap depth is limited to $10 \mu\text{K}$, according to the higher temperature of the sample. Again, the decay is nonexponential and initially about two times faster than

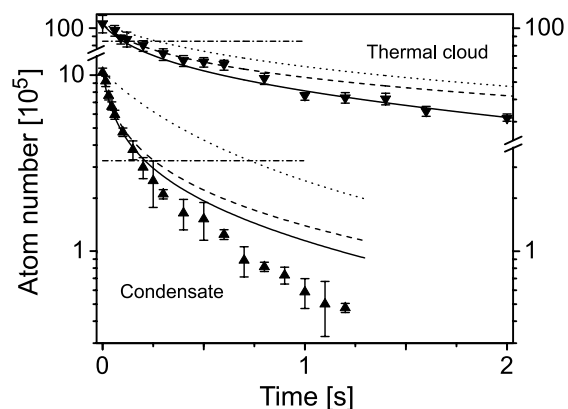


FIG. 2. Decay of the condensate and the thermal cloud. The horizontal line corresponds to the critical opacity. For comparison, the calculated decay due to the initial one-, two-, and three-body loss rates without (dotted line) and with avalanche enhancement (dashed line) are shown. The full line includes the effect of an Oort cloud with avalanche enhancement.

predicted by the primary loss rates (dotted line). At an opacity of 0.9, obtained by assuming an ideal Bose distribution, we already expect a weak avalanche enhancement. This allows us to test our model in a different regime since in a thermal cloud avalanches are less persistent than in a condensate. In addition, the intrinsic two- and three-body decay rates will die out during the observation time whereas the effect of an Oort cloud as a one-body decay will persist. The solid line in Fig. 2 is the prediction of our model where we have included an avalanche-enhanced decay rate caused by an Oort cloud. Good agreement with the data is obtained for $1/\tau = 1/7.8$ s, corresponding to $n_{\text{Oort}} = 5 \times 10^8 \text{ cm}^{-3}$ at $400 \mu\text{K}$. Such a density is produced by only a few times 10^5 atoms and appears realistic in view of the more than 10^9 atoms that were loaded into the magnetic trap. It is also consistent with the fact that we have no direct experimental evidence for an Oort cloud and that the initial decay is correctly predicted by the model even if the contribution of the Oort cloud is neglected (dashed line).

We can now calculate the extra loss rate of the condensate due to an Oort cloud. Since the two experiments described above are performed under identical conditions, the density of the Oort cloud is essentially unchanged in the two measurements. As can be seen from the solid line in Fig. 2, the small extra contribution from the Oort cloud does not change the predicted initial decay, but slightly improves the agreement between the model and the data for longer times. The small remaining discrepancy can be the result of an additional decay not accounted for in our model. In particular, avalanches will seriously perturb the equilibrium of the condensate by inducing local fluctuations of the mean-field energy [5]. Since the damping rate of excitations can be small compared to the elastic collision rate, we expect that this process introduces a second time scale to the decay that depends on the history of the condensate.

The simultaneous agreement of our model with the two complementary data sets strongly supports the evidence for the occurrence of collisional avalanches in our experiments. Our analysis reveals that the density of a cold gas is severely limited as soon as the s -wave collisional opacity exceeds the critical value of 0.693. It is important to point out that the anomalous initial decay of the condensate is attributed to collisional avalanches almost exclusively triggered by the intrinsic process of recombination and that no free parameters are introduced in the model. We have no evidence for the contribution of an Oort cloud to the fast initial decay observed in our experiments.

We conclude that it will be hard to enter the collisional regime in alkali BEC systems. For ^{87}Rb in the $|2, 2\rangle$ state the prospects are even worse due to the large collision cross

section of the recombination products. Hydrodynamic conditions might be reached in the longitudinal direction in an extremely prolate geometry, as can be seen from Eq. (5). In the vicinity of Feshbach resonances, collisional deactivation of the highly excited molecules can also cause avalanches [7] which, in turn, might contribute to the fast decay reported in Ref. [2]. This offers a new application for a condensate of, e.g., ground-state helium atoms, where recombination is not possible.

The authors are indebted to B.J. Verhaar for providing us with the results of calculations regarding the scattering cross sections and the spin relaxation rates. H.C.W.B. gratefully acknowledges the hospitality of JILA, NIST, and the University of Colorado, Boulder.

-
- [1] S. Inouye *et al.*, Nature (London) **392**, 151 (1998); Ph. Courteille *et al.*, Phys. Rev. Lett. **81**, 69 (1998); V. Vuletić, A.J. Kerman, C. Chin, and S. Chu, Phys. Rev. Lett. **82**, 1406 (1999); S.L. Cornish *et al.*, Phys. Rev. Lett. **85**, 1795 (2000).
 - [2] J. Stenger *et al.*, Phys. Rev. Lett. **82**, 2422 (1999).
 - [3] J.L. Roberts, N.R. Claussen, S.L. Cornish, and C.E. Wieman, Phys. Rev. Lett. **85**, 728 (2000).
 - [4] E.A. Cornell, J.R. Ensher, and C.E. Wieman, in *Bose-Einstein Condensation in Atomic Gases*, Proceedings of the International School of Physics "Enrico Fermi," Course CXL, edited by M. Inguscio, S. Stringari, and C.E. Wieman (IOS Press, Amsterdam, 1999).
 - [5] D. Guéry-Odelin and G.V. Shlyapnikov, Phys. Rev. A **61**, 013605 (1999).
 - [6] H.C.W. Beijerinck, Phys. Rev. A **62**, 063614 (2000).
 - [7] V.A. Yurovsky, A. Ben-Reuven, P.S. Julienne, and C.J. Williams, Phys. Rev. A **60**, R765 (1999).
 - [8] R. Wynar *et al.*, Science **287**, 1016 (2000).
 - [9] B. Desruelle *et al.*, Phys. Rev. A **60**, R1759 (1999).
 - [10] H.C.W. Beijerinck *et al.*, Chem. Phys. **45**, 225 (1980).
 - [11] B.J. Verhaar (private communication).
 - [12] U. Ernst *et al.*, Europhys. Lett. **41**, 1 (1998).
 - [13] U. Ernst *et al.*, Appl. Phys. B **67**, 719 (1998).
 - [14] E.A. Burt *et al.*, Phys. Rev. Lett. **79**, 337 (1997).
 - [15] J. Söding *et al.*, Appl. Phys. B **69**, 257 (1999).
 - [16] Experiments at AMOLF, Amsterdam, have also revealed anomalous decay. J. Walraven (private communication).
 - [17] Rate at $E_{\text{trap}} = k_B \times 4.4 \mu\text{K}$, calculated from the measured decay rate of $1/(74 \text{ s})$ at $E_{\text{trap}} = k_B \times 7 \text{ mK}$.
 - [18] Partial rates for the release of the Zeeman (b) or $2 \times$ Zeeman (c) splitting energy and the hyperfine (d) or $2 \times$ hyperfine (e) splitting energy.
 - [19] B.D. Esry, C.H. Greene, and J.P. Burke, Phys. Rev. Lett. **83**, 1751 (1999).
 - [20] D. Comparat (private communication).

Optical Kaleidoscope Using a Single Atom

P. Horak and H. Ritsch

Institut für Theoretische Physik, Universität Innsbruck, Technikerstrasse 25, A-6020 Innsbruck, Austria

T. Fischer, P. Maunz, T. Puppe, P. W. H. Pinkse, and G. Rempe

Max-Planck-Institut für Quantenoptik, Hans-Kopfermann-Strasse 1, D-85748 Garching, Germany

(Received 11 May 2001; published 9 January 2002)

A new method to track the motion of a single particle in the field of a high-finesse optical resonator is analyzed. It exploits sets of near-degenerate higher-order Gaussian cavity modes, whose symmetry is broken by the position dependent phase shifts induced by the particle. Observation of the spatial intensity distribution outside the cavity allows direct determination of the particle's position. This is demonstrated by numerically generating a realistic atomic trajectory using a semiclassical simulation and comparing it to the reconstructed path. The path reconstruction itself requires no knowledge about the forces on the particle. Experimental realization strategies are discussed.

DOI: 10.1103/PhysRevLett.88.043601

PACS numbers: 42.50.Ct, 32.80.Pj, 42.50.Vk

In a variety of pioneering experiments in the past few years [1–3] it has been demonstrated and widely exploited that a single near-resonant atom can significantly influence the field dynamics in a microscopic high-finesse optical resonator. Vice versa, the light field also influences the motion of a cold atom, which leads to an intricate dynamical interplay of atomic motion and field dynamics [4,5]. As a striking example, trapping of a single atom in the field of a single photon has become feasible [6,7]. This was experimentally substantiated by analyzing the characteristics of the transmitted intensity shows very good agreement with theoretical simulations [8] of the confined three-dimensional motion of the atom in the cavity light field including friction and diffusion [9–11]. Carrying this analysis further it was even possible to associate piecewise reconstructed trajectories with recorded time-dependent intensity curves [7,12], utilizing the knowledge of the near-conservative potential. However, the reconstruction was possible only for atoms with sufficiently large and conserved angular momentum around the cavity axis and can be done only up to an overall angle and the direction of rotation. The reason was that only a single cavity mode, the TEM₀₀ mode, was used. Consequently, only a single spatial degree of freedom of the atom could be extracted directly from a measurement of the transmitted field.

In this Letter we investigate a new method to obtain two-dimensional position information on the atom using near frequency-degenerate higher-order transverse modes. Examples are the Hermite-Gaussian (HG) or the Laguerre-Gaussian (LG) modes, which possess a rectangular matrix of intensity minima and maxima or a pattern of concentric rings in the transverse plane. The atom inside the resonator redistributes photons from one mode to the other and tends to phase lock them. Moreover, it induces frequency shifts and losses dependent on its position. In total, the symmetry of the intracavity field determined by cavity and pump geometry is perturbed and characteristic optical

patterns containing information on the atomic position appear. These patterns are reminiscent of a toy kaleidoscope in which small objects in a symmetric arrangement of mirrors create images of a given symmetry. Our technique yields much more information on the atomic position and motion as compared to the single-mode case and allows extraction of the atomic position from a measurement of the field pattern.

To treat this problem quantitatively we generalize previous semiclassical models of dynamical cavity QED to include finite sets of nearly degenerate eigenmodes. For a weakly saturated atom we derive a coupled set of equations for the mode amplitudes and the atomic center-of-mass motion. To be specific, let us consider a single two-level atom with transition frequency ω_a and linewidth Γ (half width at half maximum) moving inside a high-finesse optical resonator with transversal LG eigenmodes $u_{pm}(\mathbf{r})$, where p is the radial mode index and m is the azimuthal mode index [13],

$$u_{pm}(\rho, \theta, z) = C_{pm} \cos(kz) e^{-(\rho^2/w_0^2) + im\theta} \times (-1)^p \left(\frac{\rho\sqrt{2}}{w_0} \right)^{|m|} L_p^{|m|} \left(\frac{\sqrt{2}\rho^2}{w_0^2} \right), \quad (1)$$

where L_n^α is the generalized Laguerre polynomial. The normalization parameters, C_{pm} , are chosen such that $\int |u_{pm}(\rho, \theta, z)|^2 dV = dw_0^2 \pi/4 = V_{00}$ (the TEM₀₀ mode volume), where w_0 is the cavity waist and d the cavity length. At each spatial point the local atom-mode couplings are $g_{pm}(\mathbf{r}) = g_0 u_{pm}(\mathbf{r})$, where g_0 is the maximum coupling of the TEM₀₀ mode. The electric field is given by $\sum_{pm} \alpha_{pm} u_{pm}(\mathbf{r})$, where α_{pm} is the amplitude of the mode u_{pm} . For simplicity, we assume that the mirrors are ideally spherical and have a uniform coating. Then, all these modes have a common eigenfrequency ω and field decay rate κ . However, the model can be extended to incorporate nondegenerate modes in a straightforward manner. The cavity is assumed short compared to the

Rayleigh length of the mode so that the wave fronts are approximately plane with z dependence $\cos(2\pi z/\lambda)$. The resonator is externally driven by a coherent pump field of frequency ω_p which pumps the modes with strengths η_{pm} . Assuming low atomic saturation, we can adiabatically eliminate the internal atomic dynamics and treat the atom

as a linearly polarizable particle, which induces a spatially dependent phase shift and loss. In the semiclassical limit, where we consider the center-of-mass motion of the atom classically, we can derive the following set of coupled differential equations for the mode amplitudes $\alpha_{pm}(t)$, the atomic position $\mathbf{r}_a(t)$, and momentum $\mathbf{p}_a(t)$ [14]:

$$\begin{aligned} \dot{\mathbf{r}}_a &= \frac{\mathbf{p}_a}{M}, & \dot{\mathbf{p}}_a &= -U_0 \sum_{m,n} \nabla [u_{pm}(\mathbf{r}_a) u_{pn}^*(\mathbf{r}_a)] \alpha_{pm} \alpha_{pn}^* + i\gamma \\ & & & \times \sum_{m,n} [u_{pm}(\mathbf{r}_a) \nabla u_{pn}^*(\mathbf{r}_a) - u_{pn}^*(\mathbf{r}_a) \nabla u_{pm}(\mathbf{r}_a)] \alpha_{pm} \alpha_{pn}^* + \chi, \\ \dot{\alpha}_{pm} &= \eta_{pm} + (i\Delta - \kappa) \alpha_{pm} - (iU_0 + \gamma) u_{pm}(\mathbf{r}_a) \sum_n u_{pn}^*(\mathbf{r}_a) \alpha_{pn} + \xi_{pm}. \end{aligned} \quad (2)$$

Here, M is the atomic mass, $U_0 = \delta g_0^2 / (\delta^2 + \Gamma^2)$ with $\delta = \omega_p - \omega_a$ the single-photon optical light shift, $\gamma = \Gamma g_0^2 / (\delta^2 + \Gamma^2)$ the spontaneous emission rate for a single-photon field, $\Delta = \omega_p - \omega$ the cavity-pump detuning, and χ and ξ_{pm} are Gaussian random variables which model momentum and cavity field fluctuations, respectively.

For an atom at rest one can solve Eqs. (2) for the mean stationary field amplitudes $\alpha_{pm}^{\text{stat}}(\mathbf{r}_a)$, which in a parametric way depend on the atomic position \mathbf{r}_a . We get

$$\alpha_{pm}^{\text{stat}}(\mathbf{r}_a) = \frac{\eta_{pm}^*}{i\Delta - \kappa} + \frac{iU_0 + \gamma}{i\Delta - \kappa} u_{pm}^*(\mathbf{r}_a) \mathcal{E}_0(\mathbf{r}_a), \quad (3)$$

where \mathcal{E}_0 is the electric field at the position of the atom,

$$\mathcal{E}_0(\mathbf{r}_a) = \frac{\sum_{p,m} u_{pm}(\mathbf{r}_a) \eta_{pm}^*}{(i\Delta - \kappa) - (iU_0 + \gamma) \sum_{p,m} |u_{pm}(\mathbf{r}_a)|^2}. \quad (4)$$

Note that the list of the values of the mode functions at the position of the atom $u_{pm}(\mathbf{r}_a)$ may be seen as coordinates of a vector, which can be rotated into the form $[u_{\text{eff}}(\mathbf{r}_a), 0, 0, \dots]$. Since any linear combination of the modes can be considered as a mode as well, the atom-field dynamics for an atom at rest thus reduces to the case of a single effective mode u_{eff} . This allows one to derive simple analytical expressions for the steady state. For a moving atom, this approach must be generalized, but still helps in finding analytical expressions for friction and diffusion coefficients for the atomic motion [15].

Let us now consider the family of three degenerate cavity modes with $(p, m) = (1, 0), (0, -2), (0, 2)$. Figure 1 shows the steady state field intensities for the empty cavity and for two different atomic positions. For the chosen parameters [rubidium atoms, $(g_0, \Gamma, \kappa) = 2\pi \times (16, 3, 1.5)$ MHz, $(\eta_{10}, \eta_{0-2}, \eta_{02}) = 2\pi \times (6.4, 0, 0)$ MHz, $\Delta = -2\pi \times 2.25$ MHz, and $\delta = -2\pi \times 114$ MHz, leading to $U_0 = \Delta$, $\gamma = 2\pi \times 60$ kHz] the atom distributes photons between the cavity modes and changes their relative phases in such a way that a local maximum of the spatial field intensity pattern is created near the position of the atom. By a change of the detuning between the pump laser, the cavity modes, and the atomic transition, a local minimum can also be

achieved. Figure 1 shows the effect of the atom position on the shape and overall intensity of the stationary field distribution.

This dependence of the cavity field on the atomic position suggests that measuring the cavity output field distribution yields ample information on the atomic motion. In

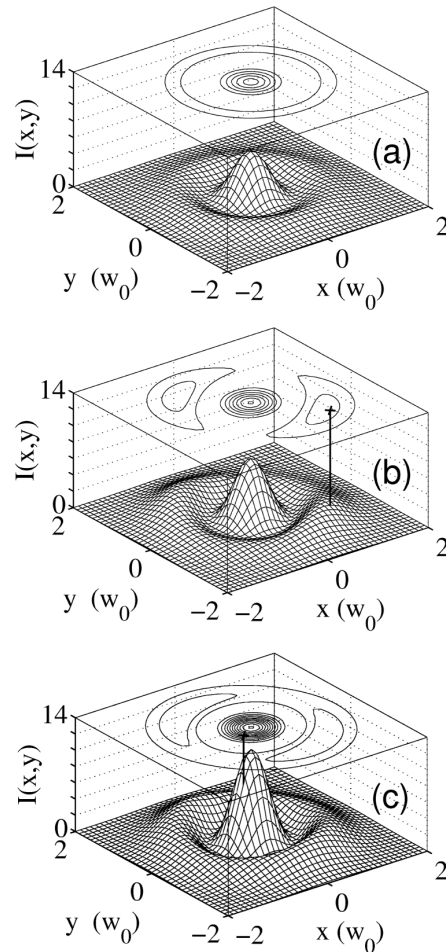


FIG. 1. Transversal spatial intensity pattern of the stationary cavity field for the empty cavity (a) and two atomic positions indicated by the thick vertical line and a cross (b), (c).

fact, it can be shown that the functions $\alpha_{pm}^{\text{stat}}(\mathbf{r}_a)$ can be inverted almost everywhere to yield the atomic position in three dimensions. Of course, one is limited by the common symmetries of all modes. For instance, for the system considered in Fig. 1, a 180° rotation around the cavity axis forms a symmetry operation. Hence, the reconstruction of the atomic position from the cavity field will always yield two equivalent positions. Other symmetry operations are a shift of $\lambda/2$ in the direction of the cavity axis and a reflection at the nodes or antinodes of the standing wave. Another limitation is that an atom cannot be detected close to the (transversal) nodes of the pumped mode (see Fig. 1a). However, it is possible to determine directly from the photodetector signals whether the atomic position can be obtained or not: reconstruction is possible if the transmission signal with an atom differs from the signal of an empty cavity. Also, the nodal areas are small and one is free to alternate rapidly between different pump geometries. Alternatively, one can change the pump geometry online when the atom approaches the nodal area of the pumped mode.

Although in principle a full three-dimensional atomic trajectory can be reconstructed, the method encounters some complications. The longitudinal motion is in general too fast to be resolved experimentally. This amounts to replacing the coupling constant g_0^2 by its longitudinally averaged value. A two-dimensional reconstruction still works in this case, even if the precise factor by which the coupling is reduced is unknown. Second, a single atom must redistribute enough photons among the cavity modes. This requires values of U_0 of the order of the cavity field decay rate κ and hence the strong-coupling regime of cavity QED. In this regime, the coherent coupling of the atom to the cavity mode is larger than the decay constants of the atomic dipole and the cavity field $g_0 > (\kappa, \Gamma)$, requiring a small high-finesse cavity. Third, our arguments above are based on a stationary cavity field. For an atom moving in the xy plane, we thus have to assume that the cavity field follows the transverse atomic motion adiabatically. This implies slow atomic motion and not too large optical forces. For strong coupling this is tantamount to low intracavity photon numbers. The limitations are strongly reduced in systems where the atom is held in place by other forces, as, e.g., in ion traps. Fourth, in an actual experiment the exact intracavity photon number can be deduced only from the number of photons emitted by the cavity, which is subject to statistical fluctuations (shot noise). These become significant in the weak field case limiting the accuracy to which the cavity field and the atomic position can be determined.

Despite all this we will now demonstrate with a realistic sample trajectory that all of these conditions can be met and a numerical reconstruction of the atomic path should be possible using existing optical resonators [6,7]. For simplicity we assume a quasi-two-dimensional situation where the atom is trapped longitudinally close to an antinode ($z = 0$) of the standing wave during the interaction time.

043601-3

In a first step we create a sample trajectory for a single atom traversing the resonator by integrating the stochastic equations of motion (2) for a given initial atomic position and velocity. This procedure includes all reactive and dissipative optical forces which the cavity field imposes on the atom [14], the backaction of the atom on the cavity field, as well as the momentum and cavity field diffusion. A resulting trajectory is depicted by the solid curve in Fig. 2. The atom enters the resonator from below. By chance, the atom encircles the cavity axis a few times before it is ejected again.

The generated trajectory allows simulation of a realistic cavity output signal. We assume an arrangement of 16 photodetectors at the cavity output port each counting the numbers of photons detected in equally sized sectors covering an angle of 22.5° . Because of the symmetry of the system, the signals from opposing detectors can be added without loss of information. We integrate the simulated photon counts at each detector over a time interval of 100 cavity decay times $1/\kappa$ to obtain the photon flux. For two out of the eight pairs of photodetectors it is shown in Fig. 3.

We will now use only the generated fluxes to reconstruct the atomic trajectory. First, for each time step we determine the most probable atomic position by a least-square comparison with a list of precalculated detector outputs corresponding to the steady-state field distribution $\alpha_{pm}^{\text{stat}}(\mathbf{r}_a)$ for given atomic positions on a discrete grid. Because of the twofold spatial symmetry, we always obtain two equivalent points in that way. From a chosen initial point we select the points forming a continuous curve as a function of time. The spatial points obtained in that way are indicated by the crosses in Fig. 2. For the pump geometry chosen here, the field has a ring-shaped field node, where the atom does not couple to the pumped

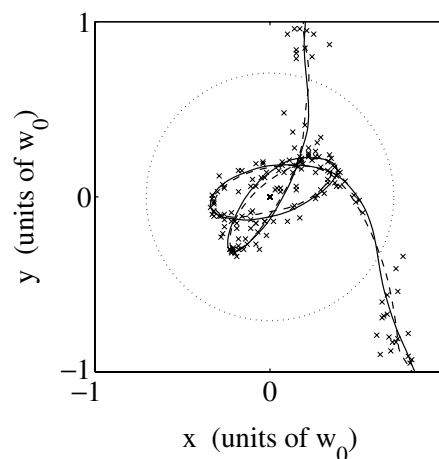


FIG. 2. Central part of Fig. 1(a) with the simulated atomic trajectory (solid curve), reconstructed atomic positions (crosses), and fitted atomic path (dashed curve). The atom enters with a velocity of 12 cm/s and the total trajectory takes $5300 \kappa^{-1} = 0.56$ ms. The dashed circle indicates the dark ring of the pumped cavity mode u_{10} . The waist of the TEM_{00} mode is $w_0 = 29 \mu\text{m}$.

043601-3

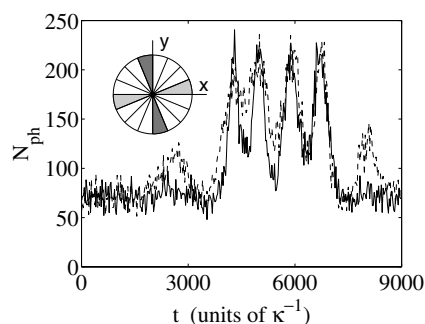


FIG. 3. Simulated photon flux (number of photons N_{ph} per $100 \kappa^{-1}$) measured at two out of 8 photodetector pairs as a function of time (units of κ^{-1}). The inset depicts the arrangement of the detectors on the cavity output, shaded areas correspond to the plotted curves.

modes. Close to this ring, the reconstruction is difficult. In principle there are ways around this problem, but here the corresponding crosses are simply left out.

Because of shot noise in the measured photon fluxes (Fig. 3), the reconstructed atomic positions show a certain spatial spread. Since for the given parameters the momentum diffusion in Eqs. (2) is small compared to the dipole force, we fit a smooth curve to the discrete set of data. The resulting reconstructed trajectory is shown by the dashed curve in Fig. 2. Note that rotation by 180° forms an equivalent solution, which can be selected by choosing an alternative initial condition. Comparing the reconstructed with the original trajectory we note that for the depicted area close to the cavity axis the reconstruction works very well with an accuracy of $w_0/30 \approx 1 \mu\text{m}$, which happens to be of the order of an optical wavelength.

The proposed detector arrangement was chosen to allow for easy analytic integration of the field intensity over the detector area and is not optimized for the best reconstruction results. It might be constructed by segment mirrors imaging onto an array of single-photon counting detectors. Direct imaging on a high-sensitive high-speed camera seems more practical. In this case one has to numerically generate the lookup table to identify the most probable atomic position for a given field distribution. The construction of a suited cavity will be challenging. Scatter, misalignment, and deformation of the high-reflectivity mirrors must be kept to a minimum to prevent breaking of the cylindrical symmetry, which could lift the frequency degeneracy of the modes by too large of an amount. In the cavity in Garching the three modes used in our numerical example lie within a range of 22κ . It seems reasonable to assume that for a specially built cavity a splitting smaller than κ is feasible.

An extension of the idea presented here is to use a cavity where modes with different longitudinal mode index are degenerate. In that case, one can choose a combination

of modes with opposite parity to break the 180° rotation symmetry. An example is a LG mode with even m degenerate with another one with odd m . Alternative geometries involving many degenerate modes as of a confocal cavity proposed in Ref. [16], will eventually lead to a single field maximum near the position of the atom avoiding ambiguities in the reconstruction.

In summary, we have shown that a high-finesse microcavity could be used as a real-time single-particle detector with high spatial resolution. In contrast to conventional single-atom detection schemes, the cavity works as a phase-contrast microscope enhanced by the inherent multipath interference of the high-finesse cavity. The method does not rely on fluorescence, and hence can also work for particles without a closed optical transition. Using larger sets of higher-order modes results in the encoding of more information in the field pattern allowing one to obtain higher resolution and track several particles. The scheme presented here could be implemented for single atoms moving in presently available high-finesse cavities, but possible applications extend beyond this system. The method should, in principle, also be applicable to large (bio)molecules in vacuum or even in solution.

P.H. and H.R. acknowledge support by the Austrian Science Foundation FWF (Project No. P13435-TPH).

- [1] H. Mabuchi, Q. A. Turchette, M. S. Chapman, and H. J. Kimble, *Opt. Lett.* **21**, 1393 (1996).
- [2] P. Münstermann, T. Fischer, P. W. H. Pinkse, and G. Rempe, *Opt. Commun.* **159**, 63 (1999).
- [3] J. J. Childs, K. An, M. S. Otteson, R. R. Dasari, and M. S. Feld, *Phys. Rev. Lett.* **77**, 2901 (1996).
- [4] C. J. Hood, M. S. Chapman, T. W. Lynn, and H. J. Kimble, *Phys. Rev. Lett.* **80**, 4157 (1998).
- [5] P. Münstermann, T. Fischer, P. Maunz, P. W. H. Pinkse, and G. Rempe, *Phys. Rev. Lett.* **82**, 3791 (1999).
- [6] P. W. H. Pinkse, T. Fischer, P. Maunz, and G. Rempe, *Nature (London)* **404**, 365 (2000).
- [7] C. J. Hood, T. W. Lynn, A. C. Doherty, A. S. Parkins, and H. J. Kimble, *Science* **287**, 1447 (2000).
- [8] A. C. Doherty, A. S. Parkins, S. M. Tan, and D. F. Walls, *Phys. Rev. A* **56**, 833 (1997).
- [9] P. Horak, G. Hechenblaikner, K. M. Gheri, H. Stecher, and H. Ritsch, *Phys. Rev. Lett.* **79**, 4974 (1997).
- [10] P. W. H. Pinkse, T. Fischer, P. Maunz, T. Puppe, and G. Rempe, *J. Mod. Opt.* **47**, 2769 (2000).
- [11] M. Gangl and H. Ritsch, *Eur. Phys. J. D* **8**, 29 (2000).
- [12] A. C. Doherty *et al.*, *Phys. Rev. A* **63**, 013401 (2000).
- [13] A. E. Siegman, *Lasers* (University Science Books, Mill Valley, CA, 1986).
- [14] P. Domokos, P. Horak, and H. Ritsch, *J. Phys. B* **34**, 187 (2001).
- [15] T. Fischer, P. Maunz, T. Puppe, P. W. H. Pinkse, and G. Rempe, *New J. Phys.* **3**, 11.1 (2001).
- [16] S. E. Morin, C. C. Yu, and T. W. Mossberg, *Phys. Rev. Lett.* **73**, 1489 (1994).

Feedback on the Motion of a Single Atom in an Optical Cavity

T. Fischer, P. Maunz, P. W. H. Pinkse, T. Puppe, and G. Rempe

Max-Planck-Institut für Quantenoptik, Hans-Kopfermann-Strasse 1, D-85748 Garching, Germany

(Received 22 January 2002; published 4 April 2002)

We demonstrate feedback on the motion of a single neutral atom trapped in the light field of a high-finesse cavity. Information on the atomic motion is obtained from the transmittance of the cavity. This is used to implement a feedback loop in analog electronics that influences the atom's motion by controlling the optical dipole force exerted by the same light that is used to observe the atom. In spite of intrinsic limitations, the time the atom stays within the cavity could be extended by almost 30% beyond that of a comparable constant-intensity dipole trap.

DOI: 10.1103/PhysRevLett.88.163002

PACS numbers: 32.80.-t, 42.50.-p

The principle of feedback is universal and finds widespread applications in science and technology. For example, feedback can stabilize a system subject to random perturbations from the environment, even in the quantum domain [1,2]. An interesting target of feedback control is the motion of a single particle such as an ion [3] or a neutral atom [4]. Here, feedback provides new avenues not accessible to, e.g., standard laser cooling and trapping techniques. In contrast to these techniques, which employ a predetermined set of operations, feedback allows one to control the particle depending on the outcome of a measurement performed on the particle. A prime example is stochastic cooling of charged particles in accelerator rings [5]. This technique has also been proposed to cool an ensemble of atoms [6] and, recently, a single trapped particle [7]. So far, feedback control of a single neutral atom has not been realized.

The key to feedback control is to observe the moving particle with high spatial and temporal resolution. High spatial resolution was achieved for a molecule embedded in a solid [8] or an ion trapped in a radio-frequency field [9]. For an atom, high spatial and temporal resolution can be obtained by placing a high-finesse optical cavity around the atom and driving the system with a laser [10,11]. If the cavity waist is small, the transmittance of the cavity depends strongly on the position of the atom [12,13]. At the same time, the intracavity light itself influences the atomic motion [14,15]. This allows one to catch an atom entering the cavity by switching the laser intensity to a higher value when the atom is detected in an antinode of the cavity mode [16,17]. The atom is then stored in the dipole trap until heating has increased its kinetic energy to a value comparable to the trap depth.

This Letter reports on feedback, applied while the stored atom moves inside the cavity. To illustrate the idea, suppose that the atom has passed the deepest point of the potential and moves uphill, thereby transforming its kinetic energy into potential energy. Most of the potential energy can be removed when the trap depth is reduced immediately after the atom has turned around. The atom will then slowly move back towards the center, where the trap depth is increased again. By repeating the sequence, and under

ideal conditions, the atom comes to a rest at the center. Such a cooling strategy requires knowledge of the velocity of the atom, which is derived from the time derivative of the position. Therefore, we call this strategy "differentiating feedback." The strategy resembles parametric cooling, but has the advantage that the modulation of the trap potential is automatically synchronized with the atomic motion. Note also that feedback cooling would be a natural extension of cavity-mediated cooling, which is caused by the delayed response of the intracavity intensity due to the high Q of the cavity [14,18,19].

Another strategy that will be presented here attacks the random momentum kicks due to spontaneous photon scattering from the trap light. These kicks disturb the otherwise regular motion of the atom in the dipole potential and lead to heating. This heating is large when the atom is in the region of high intensity at the cavity mode center. Since here the dipole force vanishes, the light field can equally well be turned off. Therefore, it is favorable to devise a trapping strategy that uses a low intensity and, hence, heats the atom only little when it is located near the trap center, but switches to a high intensity and, hence, a larger dipole force if the atom is further away. The pump power is now a direct function of the position, and we call this strategy "proportional feedback."

In our experiment, these two feedback strategies and a few deterministic strategies are implemented. The experiment is constrained by both technical and fundamental obstacles: The shot noise of the low-power ($\approx 10^{-12}$ W) light beam limits the amount of information on which the feedback can react. The random character of the atomic motion in a near-resonant light field and the shallow optical potential, which is only slightly larger than the atom's kinetic energy, impose further limits. Despite these difficulties, it is possible to extend the time an atom spends inside the cavity by means of feedback.

Our setup is similar to that described in Ref. [11]. Rubidium-85 atoms are launched towards the cavity by a pulsed atomic fountain at a repetition rate of about 0.3 Hz. On their way up, the atoms are optically pumped into the $m_F = 3$ Zeeman sublevel of the $5^2S_{1/2}F = 3$ state. The flux is kept so low that only in one out of 17 shots

a strongly coupled atom is observed in the cavity. The entrance velocities of the atoms vary between ≈ 0.08 and 0.26 m/s, depending on the arrival time in the cavity. The cavity has a finesse of 4.4×10^5 and is near resonant with the atomic transition to the $5^2P_{3/2}F = 4$, $m_F = 4$ state at a wavelength of 780 nm. Our system is characterized by half the single-photon Rabi frequency for an atom in an antinode, and the decay rates of the cavity field and the atomic dipole, $(g_0, \kappa, \gamma)/2\pi = (16, 1.4, 3)$ MHz, respectively. A circularly polarized laser pumps the TEM_{00} mode of the cavity at a rate η , normalized so that η^2/κ^2 is the mean number of photons in the resonant cavity without an atom. The frequency of the laser is tuned $2\pi \times 5$ MHz below the cavity resonance and $2\pi \times 45$ MHz below the atomic transition. For these detunings, an atom in the standing wave increases the cavity transmittance. Improving on our previous experiments [17], the cavity frequency is stabilized using a second laser resonant with a different longitudinal cavity mode at 785 nm. This light is insensitive to the presence of an atom so that the stabilization can be operated continuously. In contrast to Ref. [20], the stabilization laser is weak and does not influence the motion of the atom. The dipole force exerted by the near-resonant pump field, however, induces a fast oscillation of the atom in the direction of the cavity axis. This leads to an interesting interplay of cavity-mediated cooling and diffusion [21,22], but this is not relevant in the context of this Letter. Only the motion in the plane perpendicular to the cavity axis is slow enough to allow external feedback. In this plane, the dipole force does not change the atom's angular momentum, nor can the atom's angular position be measured. Both drawbacks can in principle be overcome by using higher order transversal modes [23].

In order to implement the feedback loop, analog electronics was set up to react on the changes of the cavity transmittance; see Fig. 1. To this end, the intensity of the light transmitted through the cavity is detected with a photon counter. The overall efficiency for detecting a photon that escapes the cavity mode amounts to about 10%.

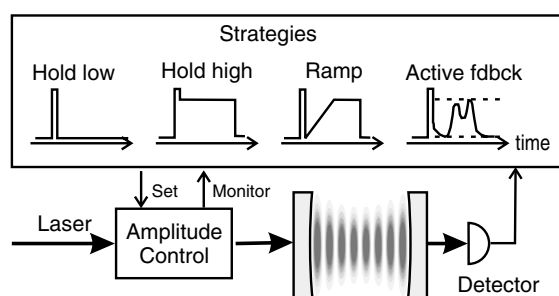


FIG. 1. Experimental setup showing the cavity and the control unit with the different strategies. “Hold low,” “hold high,” and “ramp” are deterministic. In the feedback strategies, the pump power after the initial stopping pulse depends on the motion of the atom, but is bound as indicated by the two dashed lines. The atomic fountain (not shown) injects slow ^{85}Rb atoms from below into the cavity.

The photon clicks are recorded by a computer and simultaneously sent to a count-rate-to-voltage converter (CRVC). The CRVC signal is passed through a 10 kHz low-pass filter and is used for the trigger and feedback electronics. The 10 kHz is large enough to pass the changes caused by the radial motion of the atom. The signal is then divided by the measured input power to obtain the transmittance \bar{T} . It is normalized to unity for the resonant cavity without an atom. \bar{T} depends on the atomic position and the pump power. In particular, saturation of the atom decreases \bar{T} .

Once an atom is detected in the cavity, several strategies can be applied. Each will be discussed below. They are all subject to the boundary condition that the observation light beam should not be turned off completely and that the photon detector should not be saturated. This establishes lower and upper limits for the power of the pump laser. The final signal is then sent to an acousto-optic modulator (AOM) controlling the input power. The intracavity power will follow the input power within the cavity response time, $(2\kappa)^{-1}$, which is much shorter than the time it takes an atom to travel a distance $w_0 = 29 \mu\text{m}$, the cavity mode waist.

The different control strategies are depicted in Fig. 1. Not shown is “reference,” in which we take no action other than passive observation of the passing atom. All other strategies share a fixed initial stopping pulse at a pump power of $\eta^2 = 10\kappa^2$, triggered at $t = 0$ when an atom is observed at an antinode, and has a duration of 0.15 ms which is chosen to be $\approx 1/4$ oscillation period in the dipole trap in order to remove a sizeable fraction of the atoms kinetic energy. The control strategies have a fixed maximal duration of 2 ms. They are as follows: (1) “hold low,” in which after the stopping pulse the pump power is switched to the low level $\eta^2 = 2.4\kappa^2$ that was used to detect the atom; (2) “hold high,” idem, but now the pump power is kept at a high level $\eta^2 = 7\kappa^2$; (3) “ramp,” in which the pump power is ramped up from the low to the high level in 1 ms, then remaining constant until $t = 2.15$ ms. (4) “Proportional feedback,” in which the pump power switches to the high level if $\bar{T} < 0.19$ and to the low level if $\bar{T} > 0.19$; see Fig. 2 for a typical result. (5) “Differentiating feedback,” in which the pump power is switched to the high level if the atom is seen to move away from the axis ($d\bar{T}/dt < 0$), and to a low level if the atom moves towards the center ($d\bar{T}/dt > 0$). Note that strategies (1)–(3) are completely deterministic. Strategies (4) and (5) were implemented by a proportional and differentiating circuit, respectively, reacting on \bar{T} with such high gains that the output switches between the upper or lower limit and rarely has intermediate values.

To evaluate the results, the recorded photon clicks are binned over $10 \mu\text{s}$ long intervals. The resulting signal was divided by the pump power, normalized to unity for the resonant cavity without an atom, and subsequently nearest-neighbor averaged to obtain the transmittance T . In order to determine when an atom enters and exits the cavity, T is compared with two threshold levels, L and

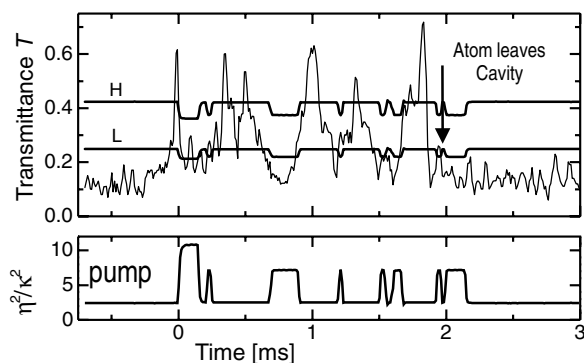


FIG. 2. A typical result for the measured transmittance, T , of the cavity (upper graph) and the corresponding pump power (lower graph) as a function of time during a proportional feedback sequence. T is large if the atom is near an antinode. The irregular behavior of T indicates the nonconservative motion of the atom. L and H are threshold levels used to evaluate the data.

H ; see Fig. 2. Level L is $1.2\times$ the empty-cavity T plus a correction that is proportional to the expected Poissonian noise. Level H is $1.7\times$ level L . It is assumed that an atom resides in the cavity if $T > H$, or if $T > L$ for more than 0.1 ms. The entrance time is set to the moment when T first exceeds L . The exit time, t_e , is defined with respect to the trigger time, $t = 0$, and is tentatively set to the moment when T drops below L . If T returns above L within 0.1 ms, it is decided that the atom still resides in the cavity. In addition, if within 0.5 ms after the tentative leave of an atom, a second signal qualifies as an atom in the cavity, it is assumed that this is the same atom returning from an excursion to the outer region of the cavity mode. The 0.5 ms interval is chosen on the basis of simulations where this near-absent behavior was observed.

In total, we have recorded several thousand events for which we determined the entrance time and the exit time, t_e . Results are listed in Table I, and three exit-time histograms are plotted in Fig. 3. The overall structure looks similar in all cases. As the initial 0.15 ms stopping pulse is not perfect, approximately $2/3$ of the atoms are not slowed down enough and, hence, can escape the cavity during the stopping pulse. The probability for an atom to stay longer defines the capture probability. It is determined for each strategy and is tabulated in Table I. It represents an average over all events, and hence, over all entrance velocities. It is observed that the capture probability is higher for the slow atoms that arrive late in a fountain shot. The capture probability is smallest without the stopping pulse, as measured in "reference." That even without a stopping pulse atoms are sometimes captured is probably due to momentum kicks by the probe light in the cavity. The random character of these kicks allows one to catch some of the slowest atoms. If a stop pulse is applied, the capture probability is much higher and independent of the feedback strategy applied afterwards. For each strategy, the mean exit time, $\langle t_e \rangle$, is determined by averaging the t_e of

163002-3

TABLE I. Number of trigger events, capture probabilities, and mean exit times $\langle t_e \rangle$ for different strategies and their standard error. The total measuring time for these 6642 trigger events is more than 100 h.

Strategy	Trigger events	Capture probability	$\langle t_e \rangle$ [μ s] 150 +
Reference	1098	0.217 ± 0.012	259 ± 19
Hold low	871	0.339 ± 0.016	298 ± 18
Hold high	1113	0.371 ± 0.015	328 ± 16
Ramp	724	0.327 ± 0.017	364 ± 33
Proportional feedback	590	0.368 ± 0.020	395 ± 23
Differentiating feedback	2246	0.340 ± 0.010	401 ± 15

the atoms that stay in the cavity longer than 0.15 ms. To exclude systematic effects, the different types of measurement were alternated irregularly during data acquisition every 1 to 2 h. No correlation is observed between capture probability and t_e .

Let us now discuss the results of the various strategies. As can be seen in Fig. 3 and in Table I, the difference between the $\langle t_e \rangle$ for hold low and hold high is only slightly larger than one standard error. To explain this, consider the ideal case for a very slow atom heading exactly towards the cavity axis and perfect timing. We express the kinetic plus potential energy of the atom, E , as a fraction of the actual trap depth $U(\eta^2)$, where the potential energy reference is the trap minimum. Ideally, the stopping pulse would reduce E/U from the initial value, $E/U(2.4\kappa^2) \approx 1$, to about $U(2.4\kappa^2)/U(10\kappa^2) \approx 0.4$ shortly after the stopping pulse, both for strategies (1) and (2). From this, and because the value of the trap depth divided by the spontaneous-emission diffusion coefficient depends only weakly on the intracavity intensity, one would expect identical $\langle t_e \rangle$. Clearly, in the nonideal case $E/U > 0.4$, as, e.g., the atoms have initial kinetic energy and angular momentum. Now E/U also depends on the final trap depth. For hold low, $U(2.4\kappa^2)/k_B = 0.16$ mK, is shallower than for hold high, where $U(7\kappa^2)/k_B = 0.34$ mK. Therefore, a somewhat

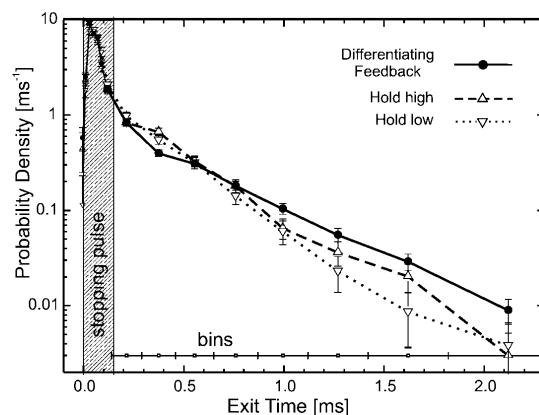


FIG. 3. Histogram of exit times. The width of the histogram bins is shown at the bottom. The hatched area indicates the 0.15 ms long stopping pulse.

163002-3

longer $\langle t_e \rangle$ for the hold high strategy as observed in the experiment seems reasonable.

An atom can escape only if its motional energy is larger than the trap depth. The former grows with the integrated heating rate, whereas the latter is only a function of the intensity at the moment of escape. Therefore, an atom can be expected to stay longer in the cavity with the strategy “ramp,” in which the pump power increases linearly after the trigger. Indeed, $\langle t_e \rangle$ for ramp is larger than that for hold low or hold high.

Let us now discuss the results of the two feedback strategies. As explained in the introduction, proportional feedback minimizes heating near the mode center while simultaneously providing a strong trapping force if the atom moves away, whereas the differentiating feedback attempts to take away motional energy of the atom. Both strategies have $\langle t_e \rangle$'s exceeding those of the deterministic strategies (1)–(3), showing that feedback can indeed be exploited to control the motion of a single neutral atom. The mechanism behind the increase in $\langle t_e \rangle$ for proportional feedback is reduced heating. The increase in $\langle t_e \rangle$ for differentiating feedback could be due to cooling, but the increase can also be accounted for by the fact that in our implementation of differentiating feedback the pump power switches to a low value if the atom approaches an antinode. The finite bandwidth of \bar{T} and, hence, the finite response time then causes the pump power to be low if the atom arrives at the antinode. This reduces momentum diffusion as in the proportional feedback strategy. As differentiating feedback does not increase the value of $\langle t_e \rangle$ beyond that for proportional feedback, cooling is not evident here.

In conclusion, we have for the first time implemented feedback on the motion of a single neutral atom, thereby extending the time the atom spends in the cavity by up to 30%. In a next-generation experiment, the laser's double function of probe and lever could be split. Two independent laser beams would allow one to optimize a near-resonant laser as a probe and a far-detuned laser as a trap. Once cooling is successful, quantization of the motion can become important. It might even be possible to cool an atom into the motional ground state. This would have many applications, e.g., in quantum information processing.

[1] Y. Yamamoto, N. Imoto, and S. Machida, Phys. Rev. A **33**, 3243 (1986).

- [2] H. M. Wiseman and G. J. Milburn, Phys. Rev. Lett. **70**, 548 (1993).
- [3] See, e.g., W. Neuhauser, M. Hohenstatt, P. E. Toschek, and H. Dehmelt, Phys. Rev. A **22**, 1137 (1980); D. J. Wineland and W. M. Itano, Phys. Lett. **82A**, 75 (1981).
- [4] Z. Hu and H. J. Kimble, Opt. Lett. **19**, 1888 (1994); F. Ruschewitz, D. Bettermann, J. L. Peng, and W. Ertmer, Europhys. Lett. **34**, 651 (1996); S. Kuhr, W. Alt, D. Schrader, M. Müller, V. Gomer and D. Meschede, Science **293**, 278 (2001); N. Schlosser, G. Reymond, I. Protzenko, and P. Grangier, Nature (London) **411**, 1024 (2001).
- [5] S. van der Meer, Rev. Mod. Phys. **57**, 689 (1985).
- [6] M. G. Raizen, J. Koga, B. Sundaram, Y. Kishimoto, H. Takuma, and T. Tajima, Phys. Rev. A **58**, 4757 (1998).
- [7] S. Mancini, D. Vitali, and P. Tombesi, Phys. Rev. A **61**, 053404 (2000).
- [8] J. Michaelis, C. Hettich, A. Zayats, B. Eiermann, J. Mlynek, and V. Sandoghdar, Opt. Lett. **24**, 581 (1999).
- [9] J. Eschner, Ch. Raab, F. Schmidt-Kaler, and R. Blatt, Nature (London) **413**, 495 (2001); G. R. Guthöhrlein, M. Keller, K. Hayasaka, W. Lange, and H. Walther, Nature (London) **414**, 49 (2001).
- [10] H. Mabuchi, Q. A. Turchette, M. S. Chapman, and H. J. Kimble, Opt. Lett. **21**, 1393 (1996).
- [11] P. Münstermann, T. Fischer, P. W. H. Pinkse, and G. Rempe, Opt. Commun. **159**, 63 (1999).
- [12] G. Rempe, Appl. Phys. B **60**, 233 (1995).
- [13] R. Quadt, M. Collett, and D. F. Walls, Phys. Rev. Lett. **74**, 351 (1995).
- [14] P. Münstermann, T. Fischer, P. Maunz, P. W. H. Pinkse, and G. Rempe, Phys. Rev. Lett. **82**, 3791 (1999).
- [15] C. J. Hood, M. S. Chapman, T. W. Lynn, and H. J. Kimble, Phys. Rev. Lett. **80**, 4157 (1998).
- [16] C. J. Hood, T. W. Lynn, A. C. Doherty, A. S. Parkins, and H. J. Kimble, Science **287**, 1447 (2000).
- [17] P. W. H. Pinkse, T. Fischer, P. Maunz, and G. Rempe, Nature (London) **404**, 365 (2000).
- [18] P. Horak, G. Hechenblaikner, K. M. Gheri, H. Stecher, and H. Ritsch, Phys. Rev. Lett. **79**, 4974 (1997).
- [19] V. Vuletić and S. Chu, Phys. Rev. Lett. **84**, 3787 (2000).
- [20] Y. Ye, D. W. Vernooy, and H. J. Kimble, Phys. Rev. Lett. **83**, 4987 (1999).
- [21] A. C. Doherty, T. W. Lynn, C. J. Hood, and H. J. Kimble, Phys. Rev. A **63**, 013401 (2000).
- [22] P. W. H. Pinkse, T. Fischer, P. Maunz, T. Puppe, and G. Rempe, J. Mod. Opt. **47**, 2769 (2000).
- [23] P. Horak, H. Ritsch, T. Fischer, P. Maunz, T. Puppe, P. W. H. Pinkse, and G. Rempe, Phys. Rev. Lett. **88**, 043601 (2002).

Deterministic Single-Photon Source for Distributed Quantum Networking

Axel Kuhn, Markus Hennrich, and Gerhard Rempe

Max-Planck-Institut für Quantenoptik, Hans-Kopfermann-Strasse 1, 85748 Garching, Germany

(Received 25 April 2002; published 19 July 2002)

A sequence of single photons is emitted on demand from a single three-level atom strongly coupled to a high-finesse optical cavity. The photons are generated by an adiabatically driven stimulated Raman transition between two atomic ground states, with the vacuum field of the cavity stimulating one branch of the transition, and laser pulses deterministically driving the other branch. This process is unitary and therefore intrinsically reversible, which is essential for quantum communication and networking, and the photons should be appropriate for all-optical quantum information processing.

DOI: 10.1103/PhysRevLett.89.067901

PACS numbers: 03.67.Hk, 32.80.Bx, 42.55.Ye, 42.65.Dr

A future quantum network connecting remote quantum processors and memories has several advantages in processing quantum information as compared to a local quantum computer, since it combines scalability with modularity. Different kinds of networks have been proposed [1]: one is an all-optical network [2], where the nodes are linear optical components, with quantum information encoded in the number of photons flying from node to node. The nodes perform gate operations based on quantum interference effects between indistinguishable photons. In another, more general, network the nodes also serve as quantum memories storing information, e.g., in long-lived states of atoms located in an optical cavity [3]. The key requirement for such a network is its ability to interconvert stationary and flying qubits and to transmit flying qubits between specified locations [4]. The atom-cavity system, in particular, must be able to transfer quantum information between atoms and photons in a coherent manner [5,6]. It must also act as an emitter and a receiver of single-photon states. These states must therefore be generated by a reversible process. However, all deterministic single-photon emitters demonstrated so far [7–15] do not meet this essential requirement. The reason is that the emission process, namely, an electronic excitation of the system followed by spontaneous emission, cannot be described by a Hamiltonian evolution and, hence, is irreversible.

This Letter describes the realization of an intrinsically reversible single-photon source [3,16–19], which is based on a stimulated Raman process driving an adiabatic passage (STIRAP) [20] between two ground states of a single atom strongly coupled to a single mode of a high-finesse optical cavity [21,22]. A laser beam illuminating the atom excites one branch of the Raman transition, while the cavity vacuum stimulates the emission of the photon on the other branch. STIRAP is slow compared to the photon lifetime in the cavity, so that the field generated inside the cavity is instantaneously mapped to the outside world. Moreover, it employs a dark state, which has two important consequences: first, any electronic excitation is avoided, so that irreversible spontaneous processes do not occur.

Second, the scheme allows one to continuously tune the frequency of the photon within a range that is only limited by the atom-cavity coupling strength. The tuning ability has recently been demonstrated with a beam of atoms passing through the cavity [23]. This experiment produced at most one photon per passing atom, but did not operate as a single-photon source, because its continuous driving scheme simply mapped the random (Poissonian) atom statistics to the photons. The present experiment, however, uses a pulsed driving together with a pulsed recycling. This makes it possible to produce on demand a stream of several single-photon pulses from one and the same atom, triggered by the detection of a “first” photon emitted from the cavity.

Figure 1(a) shows the basic scheme of the photon-generation process. A single ^{85}Rb atom is prepared in state $|u\rangle$, which is the $F = 3$ hyperfine state of the $5S_{1/2}$ electronic ground state. The atom is located in a high-finesse optical cavity, which is near resonant with the 780 nm transition between states $|g\rangle$ and $|e\rangle$. Here, $|g\rangle$ is the $F = 2$ hyperfine state of the electronic ground state, and $|e\rangle$ is the electronically excited $5P_{3/2}(F = 3)$ state. The state of the cavity is denoted by $|n\rangle$, where n is the number of photons. When the atom is placed inside the cavity, the product states $|g, n\rangle$ and $|e, n - 1\rangle$ are coupled by the electric dipole interaction, characterized by the Rabi frequency $\Omega_n = 2g\sqrt{n}$. Here, g is the average atom-cavity coupling constant, which takes into account that neither the position of the atom in the cavity nor the magnetic quantum number of the atom is well defined in the experiment. We assume g to be constant while a pump-laser pulse with Rabi frequency $\Omega_p(t)$ is applied. This laser is close to resonance with the $|u\rangle \leftrightarrow |e\rangle$ transition, so that now the three product states $|u, n - 1\rangle$, $|e, n - 1\rangle$, and $|g, n\rangle$ of the atom-cavity system are coupled. For the one-photon manifold, $n = 1$, and a Raman-resonant excitation, where the detunings of the pump-laser, Δ_p , and the cavity, Δ_C , from the respective atomic transitions are equal, it is straightforward to find the three eigenstates of the coupled atom-cavity system, $|\phi_1^\pm\rangle$ and $|\phi_1^0\rangle = [2g|u, 0\rangle - \Omega_p(t)|g, 1\rangle]/\sqrt{4g^2 + \Omega_p^2(t)}$. Note that state $|\phi_1^0\rangle$ is dark, i.e., has no

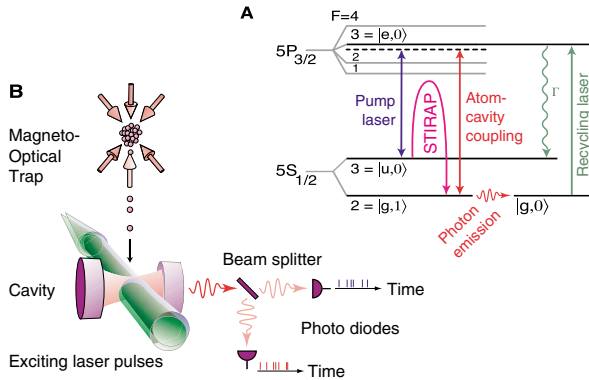


FIG. 1 (color online). Scheme of the experiment. (A) Relevant energy levels and transitions in ^{85}Rb . The atomic states labeled $|u\rangle$, $|e\rangle$, and $|g\rangle$ are involved in the Raman process, and the states $|0\rangle$ and $|1\rangle$ denote the photon number in the cavity. (B) Setup: a cloud of atoms is released from a magneto-optical trap and falls through a cavity 20 cm below in about 8 ms with a velocity of 2 m/s. The interaction time of a single atom with the TEM_{00} mode of the cavity (waist $w_0 = 35 \mu\text{m}$) amounts to about $17.5 \mu\text{s}$. The pump and recycling lasers are collinear and overlap with the cavity mode. Photons emitted from the cavity are detected by a pair of photodiodes with a quantum efficiency of 50%.

contribution of the excited state, $|e\rangle$, and is therefore not affected by spontaneous emission.

The dark state $|\phi_1^0\rangle$ is now used to generate a single-photon inside the cavity. This is achieved by establishing a large atom-cavity coupling constant, g , before turning on the pump pulse. In this case, the system's initial state, $|u, 0\rangle$, coincides with $|\phi_1^0\rangle$. Provided the pump pulse rises slowly, the system's state vector adiabatically follows any change of $|\phi_1^0\rangle$, and for a lossless cavity a smooth transition from $|u, 0\rangle$ to $|g, 1\rangle$ is realized as soon as $\Omega_p \gg 2g$. Hence, a single photon is generated in the relevant cavity mode. This photon leaves the cavity through that mirror which is designed as an output coupler. The emission starts as soon as the decaying state, $|g, 1\rangle$, contributes to $|\phi_1^0\rangle$, i.e., already with the rising edge of the pump pulse, because the contribution from $|g, 1\rangle$ is proportional to $\Omega_p^2(t)$. If the pump pulse rises slowly, the emission can therefore end even before $\Omega_p > 2g$. The dynamics of the simultaneous excitation and emission processes determines the duration and, hence, the linewidth of the photon. When the photon is emitted, the final state of the coupled system, $|g, 0\rangle$, is reached. This state is not coupled to the one-photon manifold, and the atom cannot be reexcited. This limits the number of photons per pump pulse and atom to one.

To emit a sequence of photons from one and the same atom, the system must be transferred back to $|u, 0\rangle$ once an emission has taken place. To do so, we apply recycling laser pulses that hit the atom between consecutive pump pulses. The recycling pulses are resonant with the $|g\rangle \leftrightarrow |e\rangle$ transition and pump the atom to state $|e\rangle$. From there, it

decays spontaneously to the initial state $|u\rangle$. Note that state $|e\rangle$ populated by the recycling laser couples to the cavity. However, spontaneous emission into the cavity is suppressed by deliberately choosing a large cavity detuning, Δ_C . The pump laser is detuned by the same amount to assure Raman resonance. If an atom that resides in the cavity is now exposed to a sequence of laser pulses, which alternate between triggering single-photon emissions and reestablishing the initial condition by optical pumping, a sequence of single-photon pulses is produced.

Figure 1(b) shows the apparatus. Atoms are released from a magneto-optical trap and pass through the TEM_{00} mode of the optical cavity, where they are exposed to the sequence of laser pulses. On average, 3.4 atoms/ms enter the cavity [24], so that the probability of finding a single atom inside the cavity is 5.7%, while the probability of having more than one atom is only 0.18% which is negligible. The cavity is 1 mm long and has a finesse of 60 000. One mirror has a 25 times larger transmission coefficient than the other. Therefore, photons are preferentially emitted into one direction. These photons are counted by two avalanche photodiodes which are placed at the output ports of a beam splitter. For each experimental cycle, all photon-arrival times are recorded with transient digitizers with a time resolution of 8 ns.

In the experiment, the electric field amplitudes and, hence, the Rabi frequencies of the pump and recycling pulses have the shape of a sawtooth and increase linearly, as displayed in Fig. 2(a). This leads to a constant rate of

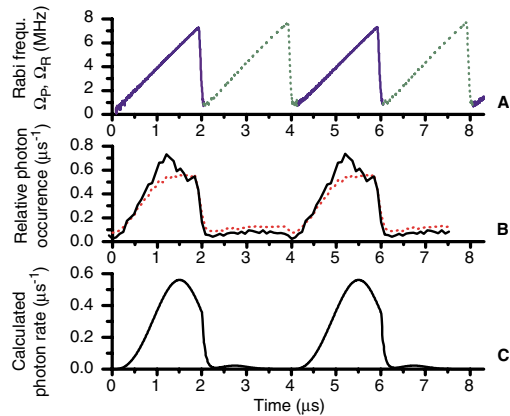


FIG. 2 (color online). Pulse shapes. (A) The atoms are periodically illuminated with 2 μs -long pulses from the pump (solid line) and the recycling laser (dotted line). (B) Measured arrival-time distribution of photons emitted from the cavity (dotted line). The solid line shows the arrival-time distribution of photons emitted from strongly coupled atoms (see text). (C) Simulation of the process with $(g, \Omega_{p,R}^0, \Delta_{p,C}, \Gamma, \kappa) = 2\pi \times (2.5, 8.0, -20.0, 6.0, 1.25)$ MHz, where $\Omega_{p,R}^0$ are the peak Rabi frequencies of the pump and recycling pulses, and Γ and κ are the atom and cavity-field decay rates, respectively.

change of the dark state, $|\phi_0^0\rangle$, during the initial stage of the pump pulses and therefore optimal adiabaticity with minimal losses to the other eigenstates. The linear slope of the recycling pulses suppresses higher Fourier components and therefore reduces photon emission into the detuned cavity. Note that the recycling process is finished before the end of the pulse is reached, so that the final sudden drop in Rabi frequency does not influence the atom.

Also shown in Fig. 2 are two measured arrival-time distributions of the photons and a simulation of the photon-emission rate for typical experimental parameters. The simulation is based on a numerical solution of the system's master equation [22] which takes into account the decay of the relevant states. The simulation [Fig. 2(c)] reveals that the pump-pulse duration of $2 \mu\text{s}$ is slightly too short, as the emitted photon pulse is not completely finished. This is also observed in the photon arrival-time distribution [Fig. 2(b)]. Here, the measured data agree well with the simulation if only photons from strongly coupled atoms are considered (solid line). For these, we assume that several photons are detected within the atom-cavity interaction time. If solitary photons, which we attribute to weakly coupled atoms, are included in the analysis, the arrival-time distribution is given by the dotted line. Note that the envelope of the photon pulses is well explained by the expected shape of the single-photon wave packets, and therefore cannot be attributed to an uncertainty in emission time, which is not present for a unitary process. Assuming transform-limited Gaussian pulses, we infer a single-photon linewidth of $\Delta\nu = 340 \text{ kHz}$ (FWHM) from the $1.3 \mu\text{s}$ photon-pulse duration (FWHM). We emphasize that the pump-pulse duration was adjusted to maximize the number of photons per atom. Longer pump pulses would not truncate the photon pulses and, hence, would slightly increase the emission probability per pulse, but due to the limited atom-cavity interaction time, the total number of photons per atom would be reduced.

Figure 3 displays an example of the photon stream recorded while single atoms fall through the cavity one after the other. Obviously, the photon sequence is different for each atom. In particular, not every pump pulse leads to a detected photon, since the efficiencies of photon generation and photon detection are limited. The second-order

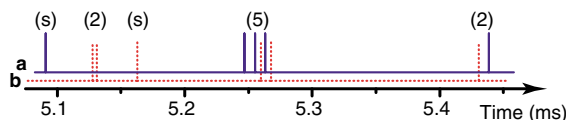


FIG. 3 (color online). Photon sequence: clip of the photon streams arriving at the photodiodes $D1$ and $D2$ (traces a and b, respectively). Several sequences of two (2) and five (5) photon emissions are observed, with durations comparable to the atom-cavity interaction time. The solitary events (s) are either dark counts, or, more likely, photons coming from atoms that are only weakly coupled to the cavity.

067901-3

intensity correlation function of the emitted photon stream is shown in Fig. 4. Displayed is the cross correlation of the photon streams registered by the two photodiodes $D1$ and $D2$. It is defined as $g^{(2)}(\Delta t) = \langle P_{D1}(t)P_{D2}(t - \Delta t) \rangle / (\langle P_{D1}(t) \rangle \langle P_{D2}(t) \rangle)$, where $P_{D1}(t)$ and $P_{D2}(t)$ are the probabilities to detect a photon at time t with photodiode $D1$ and $D2$, respectively. Note that all photon-arrival times are recorded to calculate the full correlation function, without the otherwise usual restriction of a simple start/stop measurement which would consider only neighboring events. Of course, $g^{(2)}$ includes not only correlations between photons emitted from the cavity but also those involving detector-noise counts. This last contribution has been determined from an independent measurement of the detector-noise count rate. The result is indicated by the time-independent hatched area in Fig. 4. Only the excess signal, $\tilde{g}^{(2)}(\Delta t) = g^{(2)}(\Delta t) - g_{\text{noise}}^{(2)}$, reflects the true photon statistics of the light emitted from the atom-cavity system.

The correlation function, $\tilde{g}^{(2)}(\Delta t)$, oscillates with the same periodicity as the sequence of pump pulses. This indicates that photons are emitted only during the pump pulses, and no emissions occur when recycling pulses are applied. The nearly Gaussian envelope of the comblike function is obviously a consequence of the limited atom-cavity interaction time. The most remarkable feature in Fig. 4 is the missing correlation peak at $\Delta t = 0$. In fact, photon antibunching together with $\tilde{g}^{(2)}(0) \approx 0$ is observed. This clearly demonstrates the nonclassical character of the emitted light, and proves that (a) the number of emitted photons per pump pulse is limited to one, and (b) no further emission occurs before the atom is recycled to its initial state. Note that the relatively large noise contribution is no intrinsic limitation of our system but reflects only the low atomic flux through the cavity in the present experiment.

We emphasize that the detection of a first photon signals the presence of an atom in the cavity and fixes the atom number to one. The photons emitted from this atom during subsequent pump pulses dominate the photon statistics and

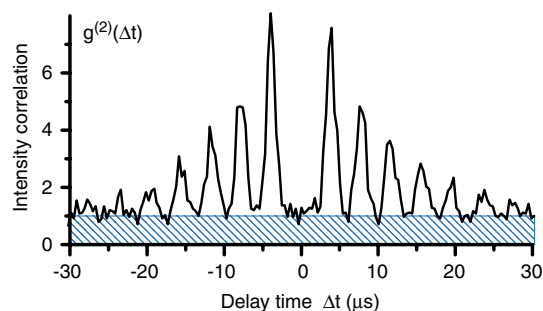


FIG. 4 (color online). Second-order intensity correlation of the emitted photon stream, averaged over 15 000 experimental cycles (loading and releasing of the atom cloud) with a total number of 184 868 photon counts. The hatched area represents correlations between photons and detector-noise counts.

067901-3

give rise to antibunching. Such an antibunching would not be observed for faint laser pulses, since a random photon statistics applies to each pulse. The areas of the different peaks of the correlation function in Fig. 4 reflect the probability for the emission of further photons from one and the same atom. They are determined from a lengthy but straightforward calculation which relates the number of correlations per pulse with the total number of photons. Using the data displayed in Fig. 4, the result for the conditional emission of another photon during the (next, 3rd, 4th, 5th, 6th, 7th) pump pulse is (8.8, 5.1, 2.8, 1.4, 0.8, 0.5)%. Note that the probabilities for subsequent emissions decrease, since the photon-emission probability, P_{emit} , depends on the location of the moving atom. It is highest for an atom in an antinode and decreases if the atom moves away from this point. It is not possible to control the atom's location in the present experiment, but it is possible to calculate $P_{\text{emit}}(z)$ from the experimental data. Here, z is the atom's vertical position relative to the cavity axis, and $P_{\text{emit}}(z)$ is averaged over all possible atomic trajectories in the horizontal xy plane. Assuming a Gaussian z dependence, the deconvolution of $\bar{g}^{(2)}(\Delta t)$ gives $P_{\text{emit}}(z) = 0.17 \exp[-(z/15.7 \mu\text{m})^2]$. For $z = 0$, the average photon-emission probability of 17% is smaller than the calculated value of 67% for an atom in an antinode of the cavity. It follows that a system combining a cavity and a single atom at rest in a dipole trap [25,26], or a single ion at rest in a rf trap [27,28], should allow one to generate a continuous bit stream of single photons with a large and time-independent efficiency [21,22]. The photon repetition rate is limited by the atom-cavity coupling constant, g , which one could push into the GHz regime by using smaller cavities of wavelength-limited dimensions in, e.g., a photonic band gap material.

In conclusion, we have shown that a coupled atom-cavity system is able to emit single photons on demand. Moreover, it is possible to generate a sequence of up to seven photons on demand from one and the same atom in a time interval of about 30 μs . These photons are all generated in a well-defined radiation mode. They should have the same frequency and a Fourier-transform limited linewidth, limited from above by the decay rate of the cavity field [23]. It follows that one can expect the photons to be indistinguishable and, therefore, ideal for all-optical quantum computation schemes [2]. Moreover, the photon-generation process is unitary. This makes it possible to produce arbitrarily shaped single-photon pulses by suitably tailoring the envelope of the pump pulse. For symmetric pulses, the emission process can be reversed. This should allow one to transfer the photon's quantum state to another atom located in another cavity. Such a state mapping between atoms and photons is the key to quantum tele-

portation of atoms between distant nodes in a quantum network of optical cavities [3].

This work was supported by the research program "Quantum Information Processing" of the Deutsche Forschungsgemeinschaft and by the European Union through the IST (QUBITS) and IHP (QUEST) programming.

-
- [1] See, e.g., C. Monroe, *Nature (London)* **416**, 238 (2002).
 - [2] E. Knill, R. Laflamme, and G.J. Milburn, *Nature (London)* **409**, 46 (2001).
 - [3] J.I. Cirac, P. Zoller, H. J. Kimble, and H. Mabuchi, *Phys. Rev. Lett.* **78**, 3221 (1997).
 - [4] D.P. DiVincenzo, *Fortschr. Phys.* **48**, 771 (2000).
 - [5] X. Maître *et al.*, *Phys. Rev. Lett.* **79**, 769 (1997).
 - [6] S. Brattke, B. T.H. Varcoe, and H. Walther, *Phys. Rev. Lett.* **86**, 3534 (2001).
 - [7] J. Kim, O. Benson, H. Kan, and Y. Yamamoto, *Nature (London)* **397**, 500 (1999).
 - [8] B. Lounis and W.E. Moerner, *Nature (London)* **407**, 491 (2000).
 - [9] C. Kurtsiefer, S. Mayer, P. Zarda, and H. Weinfurter, *Phys. Rev. Lett.* **85**, 290 (2000).
 - [10] R. Brouri, A. Beveratos, J.-P. Poizat, and P. Grangier, *Opt. Lett.* **25**, 1294 (2000).
 - [11] P. Michler *et al.*, *Nature (London)* **406**, 968 (2000).
 - [12] C. Santori *et al.*, *Phys. Rev. Lett.* **86**, 1502 (2001).
 - [13] Z. Yuan *et al.*, *Science* **295**, 102 (2002).
 - [14] P. Michler *et al.*, *Science* **290**, 2282 (2000).
 - [15] E. Moreau *et al.*, *Appl. Phys. Lett.* **79**, 2865 (2001).
 - [16] S. van Enk *et al.*, *J. Mod. Opt.* **44**, 1727 (1997).
 - [17] A. S. Parkins, P. Marte, P. Zoller, and H. J. Kimble, *Phys. Rev. Lett.* **71**, 3095 (1993).
 - [18] A. S. Parkins *et al.*, *Phys. Rev. A* **51**, 1578 (1995).
 - [19] T. Pellizzari, S. A. Gardiner, J. I. Cirac, and P. Zoller, *Phys. Rev. Lett.* **75**, 3788 (1995).
 - [20] N. V. Vitanov, M. Fleischhauer, B.W. Shore, and K. Bergmann, *Adv. At. Mol. Opt. Phys.* **46**, 55 (2001).
 - [21] C. K. Law and H. J. Kimble, *J. Mod. Opt.* **44**, 2067 (1997).
 - [22] A. Kuhn, M. Hennrich, T. Bundo, and G. Rempe, *Appl. Phys. B* **69**, 373 (1999).
 - [23] M. Hennrich, T. Legero, A. Kuhn, and G. Rempe, *Phys. Rev. Lett.* **85**, 4872 (2000).
 - [24] The flux of atoms is determined by a statistical analysis of the emitted light, with continuous pump and recycling lasers exciting the falling atoms. As the cavity acts as a detector, noninteracting atoms are ignored, so that its spatial mode structure is taken into account.
 - [25] N. Schlosser, G. Reymond, I. Protchenko, and P. Grangier, *Nature (London)* **411**, 1024 (2001).
 - [26] S. Kuhr *et al.*, *Science* **293**, 278 (2001).
 - [27] G. R. Guthörlein *et al.*, *Nature (London)* **414**, 49 (2001).
 - [28] A. B. Mundt *et al.*, e-print quant-ph/0202112 [*Phys. Rev. Lett.* (to be published)].